Additive Manufacturing of a Vehicle Brake System Component

Master degree in Automotive Engineering

José Diogo Sena Luz da Cruz Marques

Leiria, November 2020

Additive Manufacturing of a Vehicle Brake System Component

Master degree in Automotive Engineering

José Diogo Sena Luz da Cruz Marques

Project report under the supervision of Professor Maria Leopoldina Alves, and Professor Carlos Manuel Costa e Sousa from Escola Superior de Tecnologia e Gestão do Instituto Politécnico de Leiria.

Leiria, November of 2020

Acknowledgments

The present project was completed with the essential help and guidance of a select group of people who spent their time and efforts for a common goal when needed.

A special reference must be done to the guidance provided by Professor Doctor Maria Leopoldina Alves and to Professor Doctor Carlos Manuel Costa e Sousa, who overviewed the entire project always reminding me of the essential objectives and the better path to achieve them.

To the Professor Doctor and Automobile Engineering Course Coordinator Hélder Santos a special thanks for the time spent in guiding me through the entire process since the project theme selection until the project's submission.

Centro de Desenvolvimento Rápido e Sustentável do Produto team allowed for guidance during Prototype development and manufacturing, helping with material selection and component production, without them the final component would never exist. And for that a special thanks.

To my family and friends who always encouraged me and made me feel good and wiling to finish the project a very big "Thank You" for all the support and patience, given at the right time.

Alone and without the help and guidance provided by those mentioned above, the present project would never be a reality. Thanks to all.

Abstract

The present project aims to study the applicability of additive manufacturing (AM) in the automotive industry, namely, the applicability of AM in car parts production.

A commercial vehicle can be described as a set of systems, all integrated and communicating each other, with a common goal, move you from point A to point B as secure as possible. The present study focused on the manufacture by AM of a part from one of the systems integrated in the vehicle, namely a brake calliper, component of the brake system. The Selective Laser Melting (SLM) was the AM process that was used to manufacture the part.

It is important to understand that nowadays, a great level of evolution is occurring in the automotive industry. Some new technology had its origins in the racing world. Race teams lead by the big manufacturing car companies have the know-how and the opportunities to try and develop new technologies. This leads to a development in manufacturing processes associated with new components and materials. After some perfecting, the components and manufacturing techniques used in the racing industry find its way into the commercial vehicle market, leading to the endless flow of innovation that we see nowadays.

The component selected to be developed and furthermore manufactured using AM was a brake calliper, part of the braking system of a racing vehicle. The new SLM produced brake callipers will be used in the Formula Student racing platform.

Keywords: Additive Manufacturing, Brake System, Selective Laser Melting, Formula Student.

Resume

O presente projeto tem como principal objetivo estudar a aplicabilidade do processo de desenvolvimento e fabrico de um componente do sistema de travagem de um automóvel. Uma pinça de travão para ser produzida com recurso ao fabrico aditivo.

Durante a primeira fase do projeto foi efetuado um estudo associado aos processos de fabrico aditivo disponíveis no mercado atualmente, de forma a entender as vantagens e desvantagens de cada um. O processo de SLM foi selecionado como o processo a utilizar durante a produção do componente, após uma análise cuidada das alternativas disponíveis.

A segunda parte do projeto consistiu no estudo e dimensionamento do sistema de travagem do veículo. O Formula Student da equipa do IPL serviu como a base para o estudo do sistema. O monolugar está equipado com um conjunto de pinças produzidas a partir de um bloco sólido de alumínio por CNC. Durante este capítulo as forças e constrangimentos aplicados ao componente durante um cenário de travagem foram determinados.

O estudo do sistema de travagem é seguido de uma análise estática com recurso a software de simulação por elementos finitos do componente original. De forma a entender o comportamento das pinças de travagem em utilização pelo veículo do FSIP. Após esta análise inicial foi possível inferir que existe margem para melhoramento do componente caso um processo de fabrico diferente seja utilizado para a produção do componente.

No seguimento dos resultados do estudo estático do componente original, foi efetuado um estudo topológico considerando um tipo diferente de material, de forma a entender possíveis alterações geométricas a efetuar no componente. Recorrendo mais uma vez a um software de simulação por elementos finitos. Um novo design surgiu como uma possível solução para responder aos objetivos estipulados no início do projeto.

O novo componente foi extensivamente estudado com recurso ao mesmo método utilizado para estudar o componente original. Desta forma foi possível comparar resultados e determinar se o novo componente de facto representa uma melhoria em relação à pinça de travão original.

Após a validação do novo componente projetado foi-lhe atribuído o nome “Prototype 3”, e o mesmo foi produzido com recurso ao processo de fabrico aditivo selecionado anteriormente (SLM). Embora tenham existido alguns problemas associados à produção do componente, o mesmo foi fabricado validando assim a geometria modelada.

No final foi necessário efetuar um conjunto de operações após-fabrico de forma garantir as características mecânicas do componente e a sua correta integração no sistema a que se destina.

Keywords: Additive Manufacturing, Brake System, Selective Laser Melting, Formula Student.

Contents

List of Figures

List of Tables

List of Abbreviations and Acronyms

ASTM	American Society of Testing and Materials
AM	Additive Manufacturing
CDRSP	Centro de Desenvolvimento Rápido e Sustentável do Produto
CNC	Computer Numerical Control
DED	Direct Energy Deposition
DPD	Digital Light Processing
E	Energy
EBAM	Electron Beam Additive Manufacturing
EBM	Electron Beam Manufacturing
ESTG	School of Technology and Management
F	Force
FDM	Fused Deposition Modelling
FSIPL	Formula Student Institute Polytechnic of Leiria
IPL	Institute Polytechnic of Leiria
LMD	Laser Melting Deposition
LOM	Laminated Object Manufacturing
SLI	Slice Layer Interface
SLM	Selective Laser Melting
SLS	Selective Laser Sintering

1. Introduction

1.1. Context and Motivation

A constant increase in production technology through the last years has made possible an increase in material diversity used in competition vehicles. This type of vehicles beneficiate from the best materials available in the market regardless of their cost. The use of materials and fabrication processes in competition vehicles leads to a development in the processes, making them more affordable to everyday vehicles. Example of which are the vehicles that came out of production equipped with carbon fibre panels or accessories.

The Formula Student project allows for students to build and improve a competition vehicle to be used in racing against other teams. Constant improvements to the platform are done, with the intent of decreasing lap times and improving reliability. The present vehicle is equipped with an internal combustion engine producing around one hundred horsepower, inserted in a space frame chassis which has proven to be reliable in racing conditions (2014-2016). However, in this case, vehicle reliability is related with oversized components, leading to an overweight problem.

Brake callipers are a brake system part and there are four of them all around the vehicle. They allow the movement of pistons and pads that rub against the rotor leading to a decrease in vehicle speed. The present callipers were chosen from a catalogue of aftermarket components and until date have proven to be reliable. However, as time passes, components become dated and need to be replaced. With intent of updating the vehicle and reducing weight, brake callipers were selected as the component to be improved.

Wilwood manufactures the callipers in use in the Formula Student vehicle, they are known to excel in brake performance components and many race cars use Wilwood brake kits. Wilwood uses high grade materials and perfected manufacturing processes to achieve maximum performance in each component. However, in the last few years a new type of manufacturing technology has been emerging, additive manufacturing. This new technology allows for the utilization of a wide range of materials and more complex component geometries and might be a possible way of manufacturing a component with better mechanical properties and less weight, therefore improving the brake callipers in use.

Additive manufacturing is a topic containing several processes based on a layer-by- layer construction, based on a previous computer 3D model. Initially the component is designed using a computer software. After this process, the component is fabricated step by step, each step consisting in the deposition of a material layer. After all layers are completed the final component is formed.

One of the additive manufacturing processes is Selective Laser Melting, an additive manufacturing process which consists in the consecutive laser melting of powder material

layers. SLM allows for the manufacturing of complex geometries that conventional fabrication processes do not.

The powder to be melted in Selective Laser Melting defines the material of the final component. It is known that some materials are more difficult to process. For example, Titanium is a material with very interesting mechanical characteristics however it is not very used due to the difficulty associated with its processing. Other materials like aluminium are easier to process by conventional processes, however, the waste produced is considerable. SLM addresses both problems, being a process that takes advantage of the laser power to melt layers of powder, might be used in materials difficult to process and reduces the material waste, allowing for recycling.

1.2. Main Goals

The main goal of the present work is to study the applicability of an Additive Manufacturing (AM) process to manufacture a competition vehicle brake system component.

To accomplish the proposed goal, the following steps were defined:

- Bibliographic research about different brake systems, the different ways in which they can operate and their working parameters.
- Presentation of the complete brake system currently in use by the Formula Student IPLeiria.
- Bibliographic research about the different types of Additive Manufacturing processes and the materials they can use.
- Definition of operating conditions and restrains of the brake system component, both external and imposed by the system.
- Definition of the chosen AM process and the operating parameters.
- 3D Modelling and numerical analysis by the finite element method of the original brake system component to reach a new optimized component geometry.
- 3D Modelling and numerical analysis by the finite element method of the new optimized component.
- Comparison between the original component and the additive manufactured component in order to identify possible improvements that can be done to the manufactured component.

1.3. Organization

The present project is organised in several chapters. The chapter presentation order reflects the order in which the work was done.

Chapter one presents the context as well as the main goals of the project. It sets the beginning of the work to be done and the main project objectives are exposed.

Chapter two contains the state of the art. This chapter exposes the theoretical framework and a more detailed description about the origin and development of Additive Manufacturing processes. An initial description of the brake system operation and components is presented.

Chapter three presents the study of the brake system present in the Formula Student. This chapter is of great importance because it sets the loads and constrains to be applied in the component in study, resulting in a basis for the performed numerical simulation analysis.

In chapter four the original component is analysed. It is presented a description of the computer modelling process and some finite element studies that were done to understand the normal behaviour of the component in service.

Chapter five presents the prototype stage. Based on the results obtained during the third chapter, a possible alternative component starts to take shape. This chapter´s focus is the improvement of the new component, always keeping in mind the restrictions caused by the circumstances in which the component will be used.

Chapter six presents the production of the final component. This chapter contains an after-fabrication analysis and a description of the processes that might be implemented to improve final mechanical properties of the component.

The final chapter contains the main conclusions taken from each chapter allowing for the understanding of the importance of the project. A special set of word aimed for future improvements and projects are also presented.

2. Theoretical Framework

The need for stopping a vehicle came along with the ability to impel it. Through the years, with the improvement of powertrains and the ability to generate high values of torque and power, braking systems needed to be in constant evolution.

A brake is a device by means of which frictional resistance is applied to a moving machine member, to retard or stop the motion of the machine [1].

In the beginning, horses were used to move vehicles, and in a few years, the first internal combustion engines appeared. During this time mechanical brake systems were used. These systems used a mechanical link between the pedal/leaver and the component imposing friction to the wheels. The mechanism was acceptable to stop low power vehicles. However, along with the constant innovations in powertrains, there stood the need for more powerful brake systems. Hydraulic systems appeared as the biggest evolution in brake performance. From this point on, the main innovations became more focused on the components of the system.

As mentioned before, the main goal of the present project is the study and improvement of a brake calliper to manufacture it through an additive manufacturing (AM) process. The AM processes offer the possibility of manufacturing components with new materials, as well as less limitations regarding component geometry.

First and foremost, it is of extreme importance to understand how a hydraulic brake system works. This will set the mindset for understanding the importance of the component to be studied, the consequent manufacturing and geometry changes, that will take place in order to optimize the component, and to adequate the geometry to the AM process.

2.1. Hydraulic Brake System Operation

The hydraulic brake system was patented in 1924 by Malcom Loughead. The system, as mentioned before, proved to be very reliable and it can be found in use in the most different applications nowadays (motorcycles, mopeds, commercial vehicles, passage vehicles, etc…) [2].

The system is composed by the following elements:

- Brake pedal/lever
- Pushrod
- Master cylinder assembly
- Reservoir
- Hydraulic lines
- Brake calliper assembly

In a hydraulic brake system, when the brake pedal is pressed a pushrod transfers the force into a piston inside the master cylinder assembly. The movement of the piston causes the fluid in the reservoir to flow into a pressure chamber, resulting in an increase of pressure inside the brake system. The fluid is therefore forced to move in the direction of the brake callipers, inside of which there are another set of pistons which move to maintain the pressure inside the system. The second set of pistons are pressed against the sides of the brake pads (component of the brake calliper assembly) which contact directly with the spinning rotor. Subsequent release of the brake pedal leads to a decrease in the force applied to the master cylinder, decreasing the pressure in the system, therefore releasing the brake pads from the rotor.

The friction caused by the contact between the brake pads and the moving rotor generates brake torque, leading to a decrease in vehicle speed. The heat generated by the operation is partly dissipated through the brake rotor and partly conducted through the pads. The system is designed as a closed system, meaning that unless there are any leaks or losses, none of the fluid enters or leaves the system [2].

There are two main types of hydraulic brake systems:

Drum systems: The friction surface is a drum as represented on figure 2.1. Inside the drum there are two brake pads that stay still while the drum spins along with the wheels. Once system pressure increases, the brake pads are pressed against the interior of the drum leading to a speed decrease. The main material used to manufacture the drums is steel, since it is durable and able to endure the friction imposed by the pads.

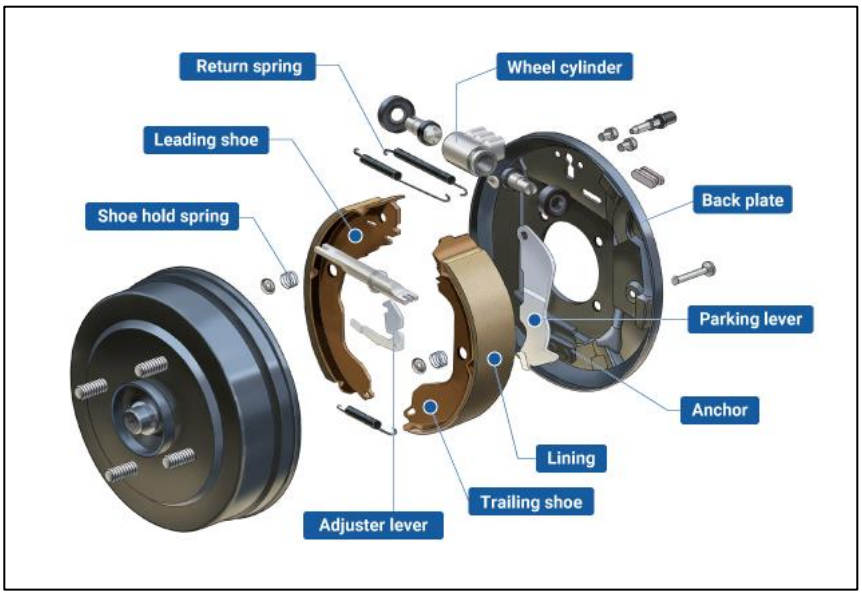

Figure 2.1- Drum brake system, adapted from [1].

However, the drum system has the disadvantage of being highly affected by external parameters (water, dust, small stones, etc). It is important to consider that the material used

in this type of system leads to a significant weight increase when compared to the disc system.

Disc system: The friction surface is a rotor attached to the wheels. The pads are located inside the brake callipers that can have one or more cylinders. The cylinders are responsible for pushing the pads against the rotor when system pressure increases. The brake rotor has two friction surfaces, one in each side of the disc (drum systems only have one friction surface). A disc brake system is represented in figure 2.2.

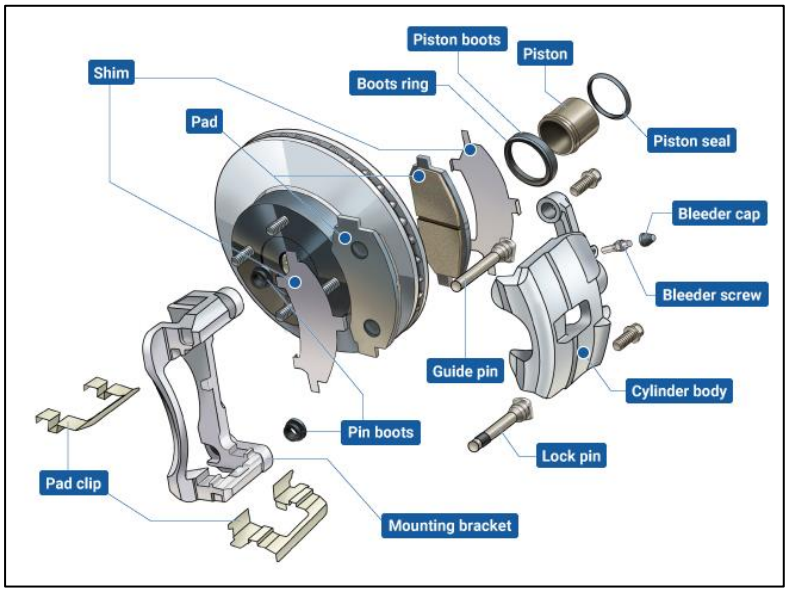

Figure 2.2- Disc brake system, adapted from [1].

There are two types of brake rotors, and each one will be actuated by a different type of brake calliper. The most common brake rotor in use in most commercial and public vehicles is the fixed rotor, floating calliper. In this type of system, the brake rotor is fixed to the wheel assembly in all directions, only allowing movement when the wheel moves. The callipers therefore need to be of floating type, and they can move perpendicularly to the friction surface of the brake rotor.

In the floating rotor fixed calliper configuration, the brake calliper is fixed, attached to the sleeve, while the rotor can move perpendicularly to the friction surface. The rotor movement and the calliper movement in both types of application should not be more than the enough for allowing the brake pads actuation.

2.1.1. The Component

As explained before there are two types of brake calliper assembly and each type will correspond to a brake rotor type. The present project intends to improve the system already in use in the Formula Student vehicle, developed in the School of Technology and Management of Polytechnic Institute of Leiria. To save time building different support parts and other assembly components, it was decided to use the same attachment points already

present in use. The assembly in use has a fixed calliper and floating rotor as shown in figure 2.3.

Figure 2.3- Brake assembly from FSIP.

The brake calliper assembly consists of the following parts:

- Brake calliper body: It allows for all the components of the assembly to stay in place while in use. The body consists in 2 different parts attached to each other.

- Brake cylinders: There are 2 equal size cylinders inside the callipers, each cylinder is contained inside the correspondent calliper part.

- O-ring: The O-ring confers a seal between the 2 body parts preventing loss of pressure or brake fluid during a braking manoeuvre.

- Square-ring seal: There are 2 equal size square-ring seals inside each half of the calliper assembly. They are placed between the slave cylinder and the calliper.

- Bleeders: There are 4 bleeders in total for each brake calliper. They allow the system to be bleed in order to maintain working parameters.

- Brake pads: Brake pads are the friction components of the calliper assembly. They are pushed by the cylinders against the rotor creating friction.

- Brake pad holders: The brake pad holders hold the brake pads in place and allow for a fast change of the braking pads if necessary.

Figure 2.4- Brake calliper assembly. Adapted from [44].

The already in use brake calliper assembly (figure 2.4) is an off the shelf product, commercialized by Wilwood [4]. Wilwood is a well renowned brand that focuses on aftermarket brake kits and components.
The "GP200 wilwood" brake calliper is fully produced using a computer numerical control (CNC) milling process from a premium grade aluminium alloy [4] and designed in order to achieve a low weight component that can be used in racing and commercial applications. During braking, the pistons inside the callipers push the pads against the disc. The forces applied to the disc by the pads leads to a reaction in the pads caused by the disc. These forces act in the opposite direction of the movement of the pistons which can lead to a separation of the brake calliper body. This phenomenon is of extremely importance and needs to be studied to achieve a new design with improved performance.

As it should be understood by now, the callipers currently in use by the formula student team are more than capable of dealing with the conditions in which they are used. However, there is space for improvement. Wildwood callipers are CNC milled, which means that they are built from a solid aluminium block, based on a 3D computer model. CNC milling has some limitations, mainly related to tool dimensions and machine characteristics which can lead to design restrictions [2].

2.2.Additive Manufacturing

Additive manufacturing (AM) started as a fast way of producing small batches or prototypes without the disadvantages related to the high production. The new manufacturing processes allowed engineers to study and develop their products without the need of using conventional manufacturing processes before final product stage. This allowed a reduction in material and costs during prototype stage.
As the years passed, additive manufacturing started to get more and more attention and the processes began to take advantage of new technology available in the market. Only a few years after its first appearance it was possible for the public to buy a 3D printer and start prototyping. However, it is important to remember that commercial 3D printers

became affordable not only by the innovations that occurred in the sector but also by the patents release that based those innovations.
The process of additive manufacturing of a component starts with the computer modelling of the desired product. The designer must consider the limitations associated with production stage (ex: dimension; tolerances, material and equipment). AM presents some advantages over more conventional manufacturing processes, however, it is not free from constrains and requires attention through all production stages. After the design stage, the component is fabricated layer-by-layer. In other words, the manufacturing process consists in the deposition of several layers of material on the top of each other to produce the desired product. This type of production is inherently less wasteful than more traditional subtractive processes and has the potential to generate economic value from the environmental impact of business activities.
Additive manufacturing has proven to be a reliable method for producing a small number of complex parts that would be very difficult to produce using conventional manufacturing processes and therefore more expensive. Many industries already produce components by AM and are constantly improving the technology to answer very specific needs. The food and Drug Administration (FDA) of USA has approved the technology for human use devices; International space station has a AM machine for producing components that can be used in space, decreasing the need of space travels; many automotive manufacturers also use AM to produce components that will be used in commercial vehicles [3].

2.2.1. Additive Manufacturing Families and Processes

Additive manufacturing can be sorted in seven different families according to the processes that lead to the final component: Binder Jetting; Material Jetting; Photopolymerization; Sheet Lamination; Directed Energy Deposition; Extrusion; Dust Fusion.

Binder Jetting: The process consists in two main stages. During 1st stage the material is applied, layer-by-layer on the build area by the coater. During 2nd stage binder material is applied over the material connecting every single material grain. After 2nd stage the building area moves and both processes are repeated until the final component is obtained. After production, the component is cleaned, and any excess material is removed to be recycled.

Binder jetting examples**:** VoxelJet and ExOne

Material Jetting: The process consists in jetting tiny droplets of liquid plastic over the build area. After a small layer is obtained, a UV light cures the plastic, solidifying it. The process will be repeated several times until the final component is obtained. Most advanced systems can build multi-material parts and adjust material properties (heat resistance or durability).

Material jetting examples: Projet and Multi-jet Modeling

Photopolymerization: This process uses a specific type of liquid resin that is located into a tank according to machine specifications. A laser unit directs a UV light beam into a reflective mirror that moves allowing the geometry to be drawn on the resin. The path drawn by the UV light in the resin becomes solid forming a layer. This process is repeated several times until the component is completed.

Photopolymerization examples: Stereolithography and DPL

Sheet Lamination: The process basis on the deposition of a solid sheet of material (metal; paper or polymer) that is cut forming a 2D layer. This operation is repeated several times as the material is glued or welded together forming a 3D object.

Sheet lamination examples: Laminated Object Manufacturing

Direct Energy Deposition : DED is a process where the metal is delivered instead of worked in a powder base. The material (powder or wire) is put in contact with an energy source (laser) in order to create a melt pool in the nozzle head. This nozzle deposits the melted material directly in a platform or part. Usually the nozzle is coupled with a CNC system which allows the formation of the desired geometry.

Direct energy deposition examples: Laser Metal Deposition

Extrusion: Process used in most commercial 3D printers. It works by depositing melted material layer by layer, through a small hole in the machine nozzle, on the top of a surface/base. The materials used are mostly thermoplastics.

Extrusion examples: Fused Deposition Modelling

Powder bed fusion: In this family of processes a layer of powder (metallic; polymeric or ceramic) is spread on the top of a moving bed and the powder is fused by a laser beam as it reaches the powder surface. After each step, a new layer of powder is spread and the process repeats until the component is completed.

Powder bed fusion examples: Selective Laser Melting and Selective Laser Sintering

Hybrid Process: This type of processes consists in the use of more than one type of manufacturing process in order to produce the finish component. One example could be the use of an additive process to obtain the part and the use of a machining process in order to finish the component. Two types of manufacturing processes were needed in order to obtain the final part.

2.2.2. Additive Manufacturing Stages

All additive manufacturing processes require a computer 3D model previous to the manufacturing stage that can be done using a variety of computer modelling programs. The 3D model file needs to be converted to a stereolithography (.STL) file, which represents the component by small triangular shapes (the majority of computer design programs have an option that allows the file to be saved in the desired format). The size of the STL file elements dictates the process precision, a bigger number of small elements will lead to a more precise 3D representation of the component.

AM processes require a geometry split layer by layer split to produce the component, and the STL file is split in layers. To achieve this goal, the STL file is converted to a Slice Layer Interface (SLI) format. The initial 3D model must take the material to be used into account, and, at this point the material should have already been selected. The next step will be the definition of production parameters according material, design, and manufacturing process. AM allows post processing operations to be performed to improve components mechanical properties and surface finish.

Additive manufacturing stages are represented in figure 2.5.

Figure 2.5- Manufacturing stages. Adapted from [4]

Layer by layer deposition presents an advantage of allowing the component to be treated as a set of 2D layers. However, 2D component sectioning leads to what is commonly known as "staircase effect". Meaning that depending on the process parameters and material, final components can present visible layers of material, as presented in figure 2.6 [5].

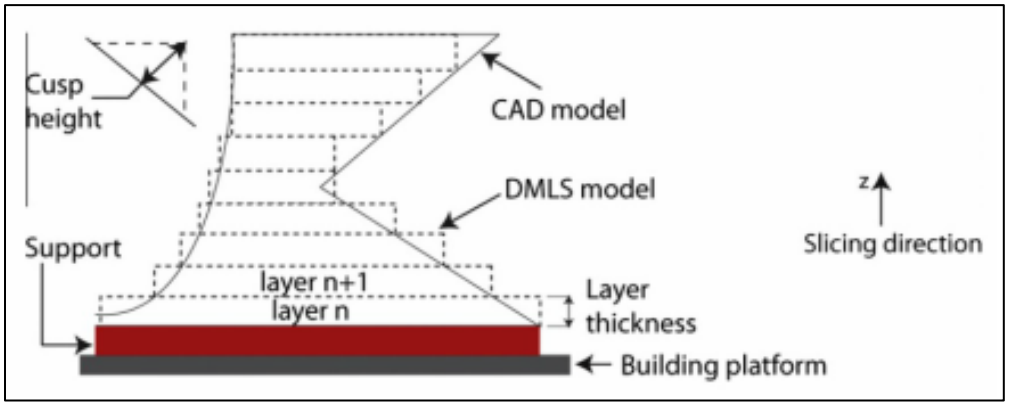

Figure 2.6- Staircase effect. Adapted from [6]

The “staircase effect” can be overcome in 2 different ways. The first solution is regarding pre-manufacturing operations:

- Computer modelling optimization.
- Material properties.
- Process and equipment parameters.

The second approach to eliminate “staircase effect” involves after-manufacturing process:

- Machining processes.
- Grinding processes.
- Coating processes.

Both solutions are applicable in solving the “staircase effect” problem. However, if the component is subjected to a post-printing process, the complete component manufacture might become an hybrid process.

2.2.3. Advantages and Limitations

Additive manufacturing, like any other manufacturing process presents advantages and limitations. The final component properties will depend on the type of process and material used.

Although some processes present specific advantages and limitations, a set of characteristics can be generalized as AM advantages:

- **Cost/Complexity relation:** Since additive manufacturing is based on a previous 3D model sliced in 2D layers, the freedom of shapes is virtually limitless. In other words, 2D layer deposition provides the user a design freedom that more conventional process cannot fulfil (ex: geometry optimization or the possibility for creating geometries that would be impossible or very expensive to produce using more common subtractive processes).
- **Assembly sets:** AM layer deposition allows the production of assembly sets, instead of the conventional individual part production. It is possible to manufacture a complete set (building area dimensions must be respected) in one manufacturing operation. This allows for a reduction in the total number of different parts and assembly costs.
- **Materials:** AM allows the use of a materials wide range, depending on the type of process to be used. Unlike conventional manufacturing processes (subtractive), AM allows the application of materials that would be very difficult to work on using other types of processes (table 2.1).
- **Design freedom:** 2D layer deposition allows the user to design a virtual limitless number of shapes impossible to recreate using more conventional manufacturing processes. For more complex shapes it is possible for the software to create support structures, to be removed after manufacturing, as shown in figure 2.7.

Table 2.1- Additive Manufacturing Material. Adapted from [8]

	Amorphous	Semi-Crystalline	Thermoset	Material Extrusion	Vat Polymerization	Material Jetting	Powder Bed Fusion	Binder Jetting	Sheet Lamination	Direct Energy Deposition
ABS	X			X						
Polycarbonate	X			X						
PC/ABS Blend	X			X						
PLA	X			X						
PEI	X			X						
Acrylics			X		X	X				
Acrylates			X		X	X				
Epoxies			X		X	X				
Nylon		X					X			
Neat		X					X			
Glass filled		X					X			
Carbon filled		X					X			
Metal filled		X					X			
Polymer bound	X	X		X						
Polystyrene	X									
Poliester							X			
Chocolate		X		X						
Paper									X	
Aluminuim							X	X	X	X
Co-Cr alloys							X	X		X
Gold							X			
Nickel alloys							X	X		X
Silver							X			
Stainless steel							X	X	X	X
Titanium							X	X	X	

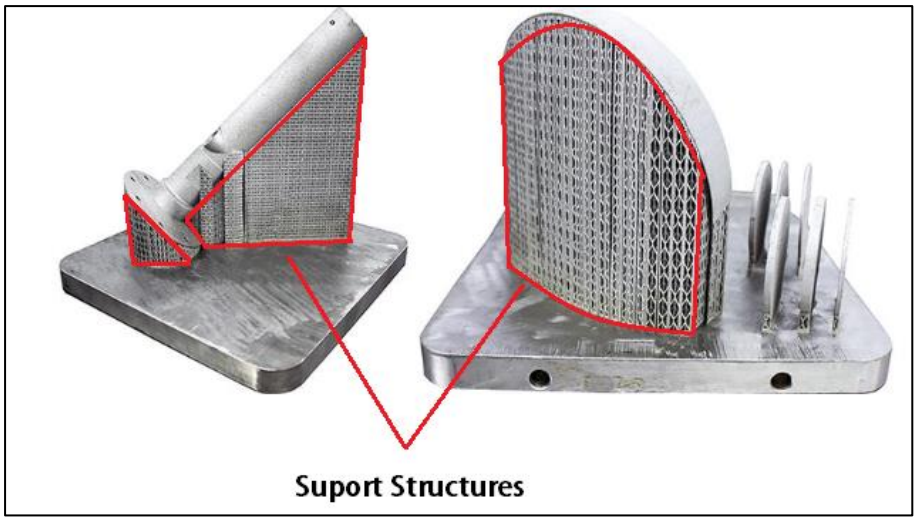

Figure 2.7- Support structures in Selective Laser Melting. Adapted from [7]

It is important to keep in mind that additive manufacturing, as other manufacturing processes, presents limitations.

The following additive manufacturing characteristics are presented as process limitations:

- **Production time:** Additive manufacturing is a time-consuming process, depending on the component dimensions and the process used, with the manufacturing process taking until a few days. Pre-manufacturing processes also take more time than conventional methods, computer modelling and the set-up phase must be optimized to obtain the best results.
- **Size limitations:** AM only allows manufacturing inside the building area, meaning thar for each AM process there are dimensional constrains that can not be exceeded, otherwise the component can not be produced.
- **Precision:** In some cases, layer by layer deposition introduces precision errors, meaning that the final component needs to go through post processing processes to improve surface quality.
- **Large scale costs:** As AM processes are more time consuming than conventional manufacturing process, the costs associated increase. This characteristic is enhanced in large production batches.

2.2.4. Metal Additive Manufacturing

Metal additive manufacturing processes allow the production of components using, as the name indicates, metallic alloys. In this type of processes, small metallic particles are used to form a new part.

The most significant metal additive manufacturing processes are as follows:

- **Binder Jetting:** This type of process uses a powder bed. An inkjet printer head is used to spread a liquid binder onto the powder after each layer of powder deposition as shown in figure 2.8. The process is repeated until the part is completed. The

process does not require heat to bind the material, however, the new metal component needs to be sintered afterward.

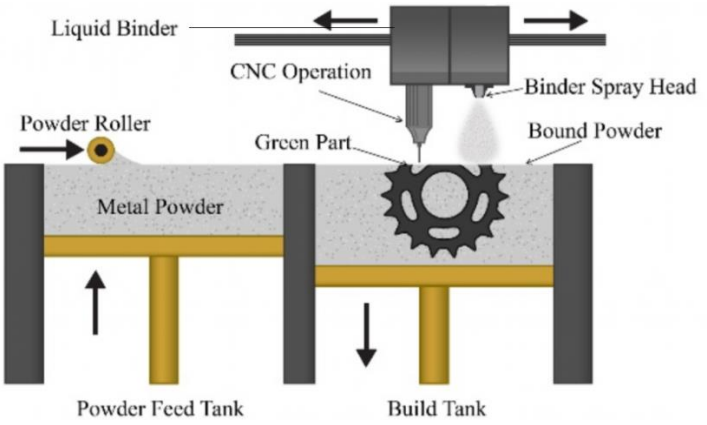

Figure 2.8- Binder Jetting, adapted from [9].

- **Nanoparticle Jetting:** In this type of process the print head deposits a fine layer of metal liquid droplets on the building tray. Temperatures can reach up to 300ºC leading to the liquid evaporation around the metal particles. A sintering process is required after printing. The process is illustrated in figure 2.9.

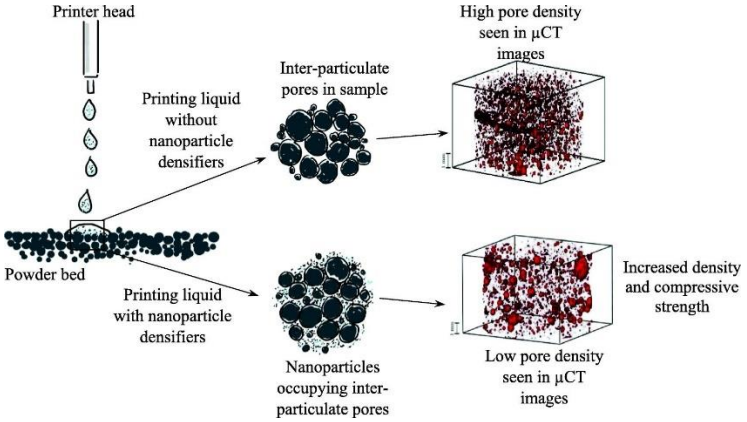

Figure 2.9- Nanoparticle Jetting process, adapted from [10].

- **Electron Beam Additive Manufacturing:** Metal is deposited directly into the component, layer by layer, from wire feed stock. A dual wire feed system can be used to increase productivity. The final component might require a post processing operation, for example a machining operation. The process is illustrated in figure 2.10.

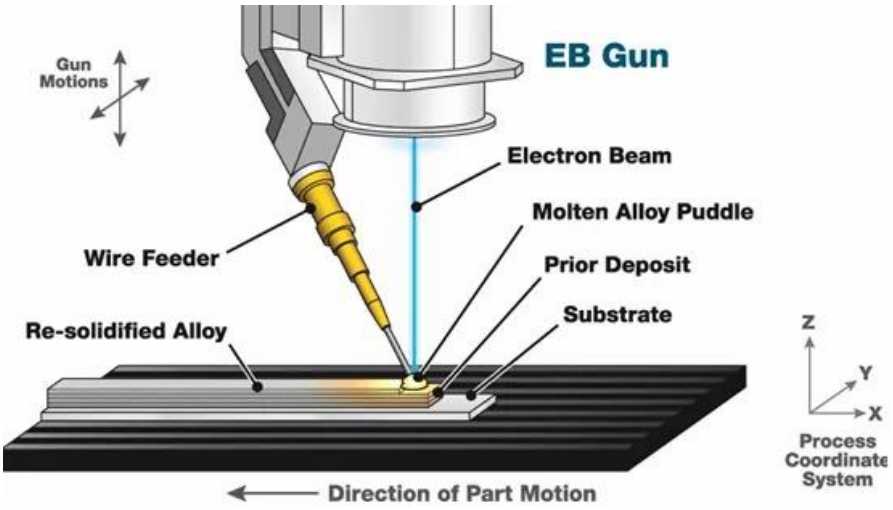

Figure 2.10- Electron Beam Additive Manufacturing process, adapted from [11].

- **Sheet Lamination:** This type of process consists in the deposition of metal, layer by layer, being trimmed and adjusted in between layers as presented in figure 2.11. After all layers are linked together, the part is completed.

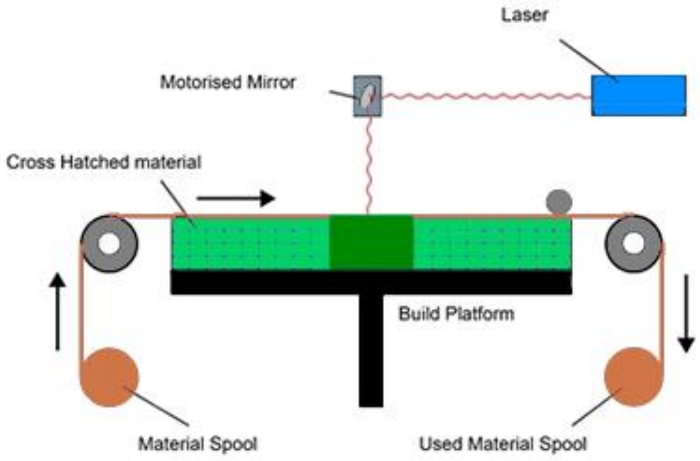

Figure 2.11- Sheet Lamination process, adapted from [12].

- **Electron Beam Manufacturing:** It is a type of powder-based print system that uses a powerful electron beam to melt the powder (contour melting, hatch melting) layer by layer. The electron beam unit allows a fast and accurate beam control. The equipment is shown in figure 2.10.

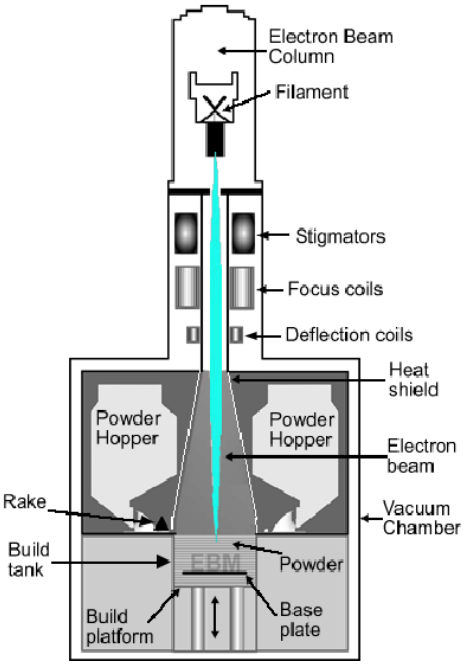

Figure 2.12- Electron Beam Manufacturing process.

- **Selective Laser Melting:** This is a type of manufacturing process similar to Electron Beam Manufacturing. The metal powder is melted, layer by layer, to produce the final component. SLM is one of the most appealing metal additive manufacturing process available today. There is a wide range of materials that can be processed using this technology which makes it ideal for rapid prototyping and mass production. This type of process will be explored in chapter 2.2.5. Figure 2.11. illustrates the equipment used for SLM.

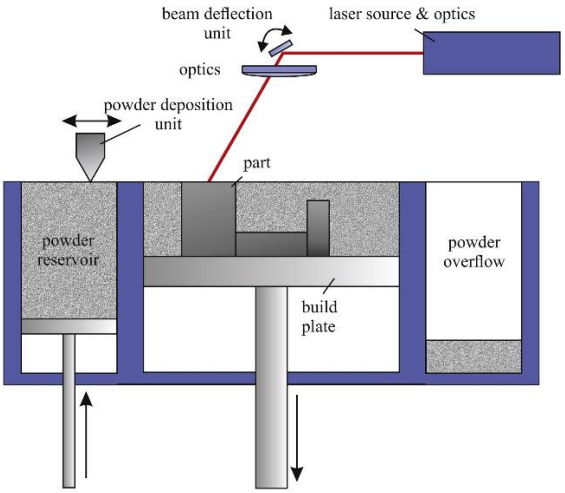

Figure 2.13- Selective Laser Melting process [13].

2.2.5. Selective Laser Melting

Selective Laser Melting is a type of powder bed fusion process. The process consists in the selective fusion of powder metals using a laser beam, layer by layer, to produce the final component.

Selective Laser Melting is an iteration derived from SLS technology. Selective Laser Sintering is a type of additive process which consists in the melting of powder material, typically polyamide or nylon by a laser, layer by layer to achieve a final component.

In SLM the metallic powder is heated above the fusion point (melting), fusing the particles together into a solid form. SLS is mainly used to process polymeric materials, while SLM can process a wide range of metals. One of the main differences between both processes is that in SLM the material is heated above the melting point, while in SLS the powder is not fully melted, reaching only sufficient temperatures to partial fuse the powder (sintering).

The SLM equipment includes a chamber, filled with metal powder that is gradually spread over the building plate in very thin layers by a roller blade. The powder is fused using a high- power laser in a 2D slice of the part selectively melting the powdered material. The building plate moves down to allow the roller to deposit another thin layer of powder. The process is repeated until the final component is achieved, figure 2.14.

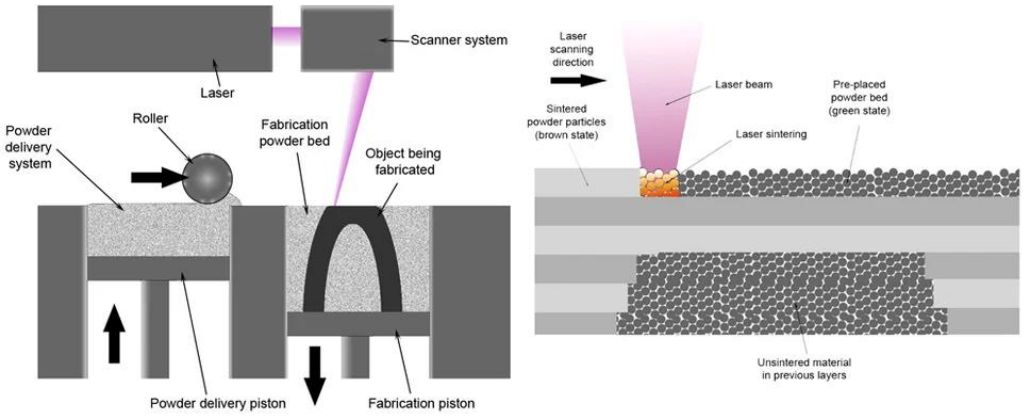

Figure 2.14- SLM, inside the machine process, from [14].

The process uses an inert gas (Argon) to control/avoid oxidation and promotes expelling fumes generated during the metal melting stage.

The powder: The size of the powders used in SLM have an average diameter of 20 to 45 µm. This powder is spread over the building platform by the roller and melted layer by layer. In between each layer of powder deposition, the building table moves down between 25 to 50 µm. The process is repeated until the final component is achieved. SLM technology uses a

wide range of metallic materials: Al-based alloys; Ni-based alloys; Ti-based alloys; Co-based alloys; Fe-based alloys; Cu-based alloys [14].

The laser: The laser beam allows to selectively melt the material to form solid layers from the powder. The light is produced in laser units generally located in the machine lower part. It is then guided to the optical unit throw fibre optic cables. The laser´s width is continuously optimized by the optical unit through movable lenses. Inside the scanning head two adjusting mirrors control the direction of the laser allowing the beam to be directed to the building chamber where it melts the metal powder.

In order to obtain final components according to the initial model dimensions and to minimize components porosity a careful configuration of the manufacture parameters is required.

The most influent parameters in the material structure are laser power and scanning speed. Melting temperature defines the amount of liquid phase in the metal components which is further influenced by the energy transferred to the powder. Both laser power and scanning speed influence the energy transferred to the powder, as shown in equation 2.1 [15].

$$E_D = \frac{P}{e.h.v} \tag{2.1}$$

- P (W): Laser beam power.
- e (mm): Powder layer thickness.
- h (mm): Space between each coater.
- v (mm/s): Laser beam speed.

Depending on different combinations of laser power and scanning speeds the SLM process can be divided in four different cases, where each case presents different material mechanical properties [15].

I. No melting: The laser beam has insufficient energy to melt the powder material, therefore, a large amount of powder remains in its initial state.
II. Partial melting: A liquid phase on the particles' surface is formed due to a combination of medium laser beam performance and low scanning speed (<0.06 m/s).
III. Melting with balling phenomenon: A higher laser power and scanning speed are used when compared to the partial melting phase, leading to the formation of long, thin cylindrical lines which later split into rows of coarse beads. Indicating that the parameters are still inadequate.

IV. Complete melting: Permanent tracks of molten material are created indicating a great laser energy. Lines are formed from the fully melted material forming a compact solid surface.

The different stages can be observed in figure 2.15.

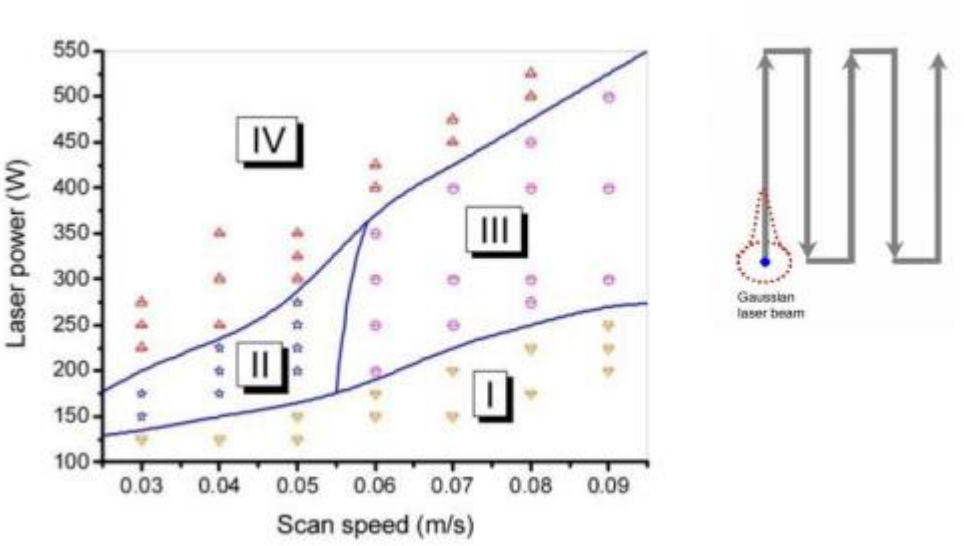

Figure 2.15- SLM mechanical properties parameters, adapted from [15].

The results shown above regarding the combinations of laser power and scanning speed were demonstrated using stainless steel 316L with a layer thickness of 20μm according to D .Gu and Y .Shen [16].

Another important factor to consider in SLM is the hatch angle. The hatch angle is the angle between laser scanning directions on consecutive layers of powder deposition. It means that, using a hatch angle of 120º, the fourth row of deposition will be equal to the orientation of the first layer rows (as represented in figure 2.16).

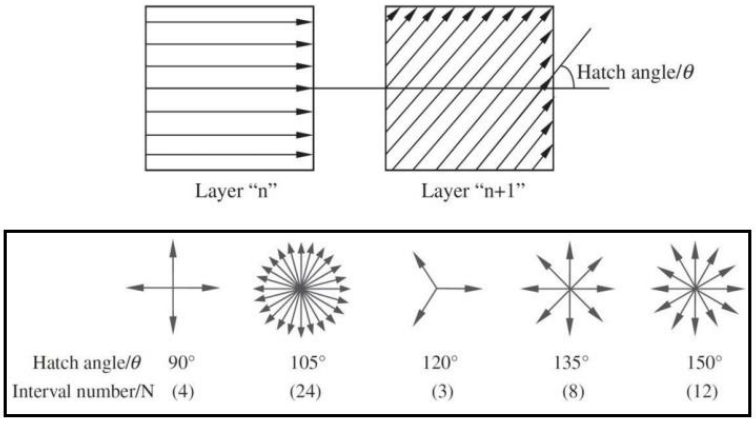

Figure 2.16- Hatch angle and interval number, adapted from [17].

According Kay Guan *et al*. [16] the selection of an unsuitable hatch angle can lead to a poor construction quality of the manufactured components. During the study, samples of stainless steel 304 built using the same laser power and scanning speed were investigated. See table 2.2 for SS-304 SLM built samples parametrization.

Table 2.2- Parameters for SLM manufacturing of SS-304.

SLM parameters for SS-304 hatch angle analysis	
Laser power	200 W
Scanning speed	0.25 m/s
Layer thickness	20 µm
Overlap rate	40 %
Building direction	0º
Hatch angle	90º; 105º; 120º; 135º; 150º

According to the properties of investigated samples, the units built using a 105º hatch angle presented the most satisfactory mechanical properties in many applications. During the study, a relation between the hatch angle and the mechanical properties was found (Table 2.3).

Table 2.3- Mechanical properties of SS-304 depending of hatch angle.

Hatch angle (º)	σ 0.2 (MPa)	UTS (MPa)
90	530-551	696-713
105	566-570	714-717
120	540-545	682-685
135	541-556	691-693
150	534-555	698-703

2.2.6. SLM vantages and limitations

Selective Laser Melting, like all AM processes, presents advantages and limitations. It is important to remember that it is a relatively new process in constant development, therefore constant improvements are being made to maximize its potential as a manufacturing process.

SLM advantages are as follows:

- Large range of metals available for use with the process
- Relatively low cost of the process
- Optimized designs to reduce the need for assembly
- Ability to manufacture complex shapes and internal features
- Ability to produce multiple parts at the same time

SLM limitations are as follows:

- Specialized knowledge and skills required
- Relatively small print area depending on the equipment
- Rough surface quality
- The process might be expensive if the component is not optimized for production

- Post-printing operations required

SLM is a high-potential technology being used in many applications. As the technology grows, the process and material become cheaper and it should become more and more widespread [14].

2.2.7. Balling phenomena

During the SLM process, while the melting track is created by the laser melting the powder, a shrinking tendency occurs to decrease surface energy due to surface tension. According to Gu. D and Yifu. S, in this condition, the balling effect can easily occur influencing thermodynamic and kinetical characteristics during powder melting stage, resulting in the formation of discontinuous melted tracks [18].

When production parameters are not set up properly the powder is either not fully melted or completely melted, forming large drops that quickly increase in size, leading to the formation of a large droplet with size that can exceed laser diameter. This phenomenon described by Tolochko et al. is called balling [19].

The balling phenomena leads to disadvantageous effects in process and component quality that can be summarized as follows:

- Increase in surface roughness leading to an increase in post-production operations, leading to a more time-consuming process.
- Increase in component porosity leading to poor mechanical characteristics of the final component.
- Severe cases of balling can lead to an obstruction to paving roller movement, scratching the component and in extreme cases to production stoppage.

Balling effect is not yet fully understood, the formation process and influencing factors are extremely complex and not clear. Previous studies have been written in the scope of Balling phenomena during SLM. Tolochko *et al*. and Gu *et al*. pointed out that balls can be divided in two types: Ellipsoidal Balls and Spherical Balls, as presented in figure 2.17.

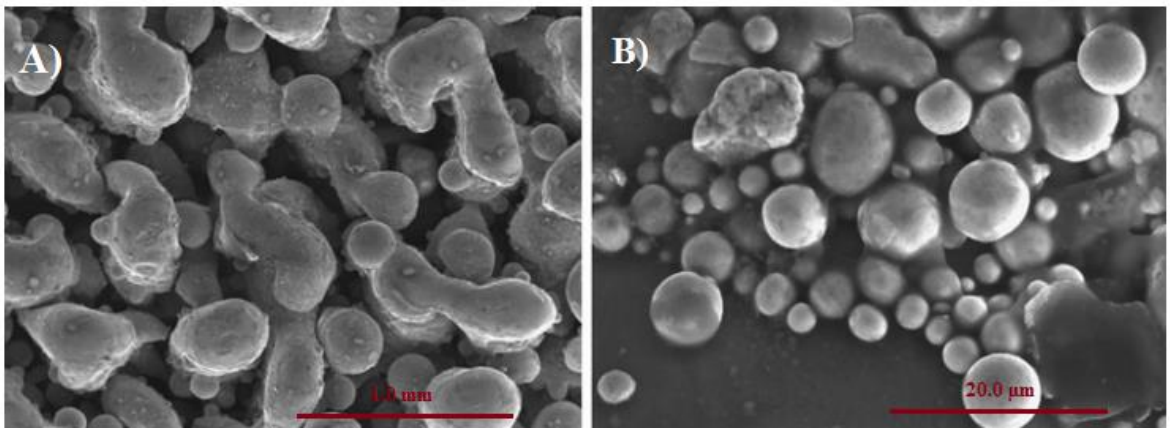

Figure 2.17- A) Ellipsoidal, big size balls B) Spherical, small size balls. Adapted from [20].

The formation of small balling (spherical balls) during the SLM process can be considered as universal. This type of balling will not interfere with the powder paving process, thus the negative impact of small size balling can be ignored. On the other hand, the formation of big size balls (ellipsoidal balls) can block the powder paving process, leading to component damage and in extreme cases, process stoppage.

The balling phenomena can be reduced by reducing the oxygen content in SLM atmosphere. According to Ruidi Li *et al*. during the process of selective laser melting powders of stainless steel and nickel based alloys, on an atmosphere with an oxygen content of about 0.1%, a smooth melting surface is created without balling initiation [20].

Regarding laser power and scanning speed, both parameters must be carefully adjusted to avoid balling formation. The relation between high laser power and low scanning speed presents a beneficial continuity in powder melting stage without balling initiation [20]. During the powder melting stage, the relation between laser power (P) and scanning speed (v) can be estimated by a single parameter, the linear energy density (λ) as presented in equation 6.1.

$$\lambda = \frac{P}{v} \tag{6.1}$$

According to equation 6.1 either an increase in laser power or a decrease in scanning speed will lead to an increase in energy density, thus increasing the temperature during melting stage. Leading to a large amount of liquid phase with a lower viscosity that spreads to surrounding unmelted solid particles. During this scenario, the liquid spreads and flows more easily reducing the chances of balling initiation [16].

During powder melting stage, thickness of powder layer has a great influence in balling formation. From an energy density viewpoint, it is possible to notice that an increase in layer thickness can lead to a decrease in laser intensity per melted volume [16]. “Volumetric energy density (VED)” relates laser power (P), layer thickness (d) and scan line spacing (h) as presented in equation 6.2.

$$VED = \frac{P}{v.h.d} \tag{6.2}$$

According to equation 6.2 an increase in layer thickness (d) while maintaining the remaining parameters will translate in a volumetric energy density decrease, leading to the initiation of balling phenomena.

The balling phenomena can also be decreased by remelting the surface of the component, leading to the melting of previously formed balls.

2.2.8. SLM over other AM processes

As shown until this point, SLM technology presents a set of appealing characteristics which make the process an interesting technology for the manufacture of metal components. However, it is important to remember that other AM processes are available in the market, competing with SLM technology.

Binder Jetting comes as an alternative to SLM, allowing a "cleaner" process. The absence of a melting stage leads to a more energy efficient process with 100% recyclable powder and no wrapping areas in the final components. However, the same lack of a melting stage leads to a final part with less strength.

Nanoparticle Jetting allows the production of a high resolution and density component, reducing the need for post-production processes (ex: machining, sintering). On the other hand, the process is relatively new in the market, leading to a low range of metallic materials available and a high production cost.

Electron Beam Additive Manufacturing is one of the fastest and most cost-effective Additive Manufacturing process in the market for producing metal parts. It has the widest range of commercial-available metal Additive Manufacturing systems allowing the use of a dual feed system for a dual material melting pool. However, the low accuracy of EBAM requires the final components to go through a wide range of post-production processes, increasing production time and costs.

Sheet Lamination allows a fast production time and is relatively cost-effective. The process does not require support structures and the construction platform is significantly larger when compared to other AM processes. However, the process has a limited material selection, layer thickness can only be altered by changing the sheets and the waste can be significant.

After analysing the most prevalent metal additive manufacturing processes, Selective Laser Melting was chosen to produce the final component in the aim of the present project. The ability to produce complex shapes and internal features (impossible to achieve via conventional manufacturing), produce several parts at the same time and manufacture components using a large range of materials make the SLM process stand out from the rest of the metal AM processes.

3. Brake System Study

The sizing of a competition vehicle brake system is a very complex study. The system is comprised of many parts including a master cylinder, calliper and brake lines. It is essential that all the variables considered match the real-life conditions to obtain the best results possible.

In the type of vehicle to be studied all four wheels are outside of the body as shown in figure

3.1. This characteristic expose some of the brake system components to advert conditions such as water and dust from the road.

Figure 3.1- Formula Student, IPLeiria.

The main goal is to obtain a high-performance brake system that can provide great stopping power to the vehicle, considering the conditions in which it will operate. The single seater will operate in a closed track reaching speeds up to 100 km/h and each race should not exceed de duration of 20 min.

The single seater already has a functioning brake system that allows for the vehicle to stop and reduce speed on demand. However, this system was applied without any previous study. Most of the components used are off the shelf components that were put together by the students in a short period of time to meet competition deadlines.

In the following pages the components and forces applied to the braking system are going to be analysed to identify possible improvements.

To compute the variables, Maple software was used. Maple software is a powerful calculator that allows changes in the variables to obtain different results. This provides the opportunity of trying different values associated with different components to compare results and chose the ones more suitable for each situation.

3.1. Forces Applied to the System

As the vehicle moves through the road a group of forces are applied to it, dictating the behaviour during acceleration, cornering and braking. This rule applies to all road vehicles with the difference being in the magnitude of the forces that can change according to vehicle size, tires, and physic characteristics. In this case the focus is going to be on the braking used at the Formula Student Single Seater vehicle.

The forces considered are shown in image 3.2.

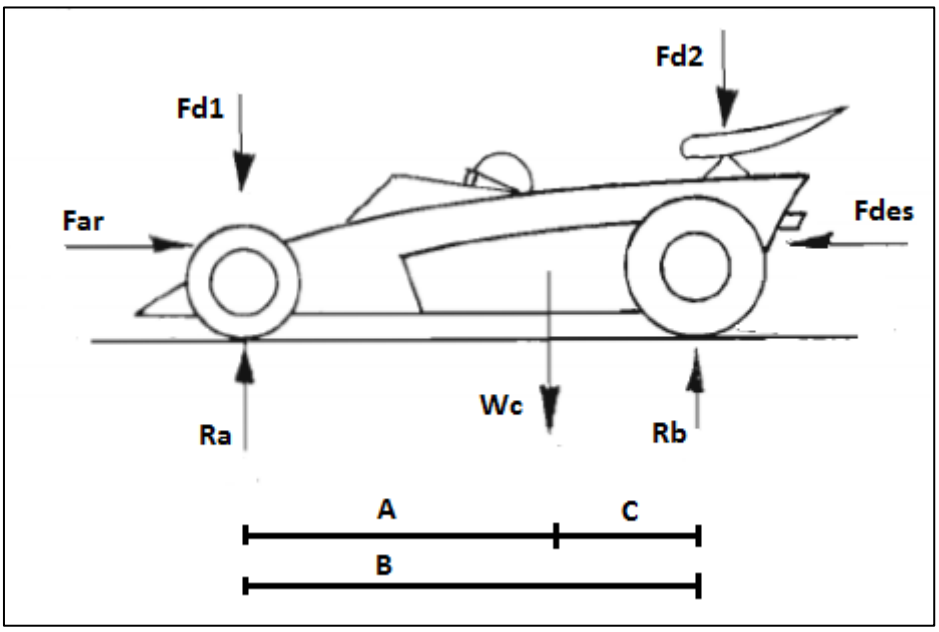

Figure 3.2- Forces applied to the system

The vehicle has two wings that provide downforce while traveling at high speed, a front and a rear one. The force provided by the wings is represented as F_d. There is also a force with opposite direction of the movement of the vehicle represented by F_{ar} corresponding to the air force, actuating on the vehicle while it moves. The weight of the vehicle is represented as W_c and applied on its mass centre. Contact points with the road are 4 tires, where the forces R_a and R_b act. Finally, A, B and C correspond to the distances between the front wheel and mass centre (A), the front and rear wheel (B) and the mass centre and rear wheel (C).

The magnitude of the downforce applied by the front and rear wings can be changed by altering the wing's surface angle, using different shape wings. During calculations it was defined a shape and area for both wings to obtain estimated downforce values. However, the values can be altered if the wings are changed or modified.

3.2. 1st Approach

The first approach consists in the study of the braking system considering maximum disc pressure without wheel slide occurring.

The data used in this chapter is based on already existing values associated with the single seater, obtained from wind tunnel simulations, and this data are shown in table 3.1.

Table 3.1- Data from formula student

Variable	Value (unit)
Air density (ρ)	1.225 kg/m^3
Velocity (v)	100 km/h
Front wing's projected area	0.2 m
Rear wing's projected area	0.4 m
Front wing's lift coefficient	0.8
Rear wing's lift coefficient	0.4
Drag coefficient	0.4

It is important to notice that there are 2 different values for the projected area and lift coefficient, these values are associated with the front and rear wings. As said before, the vehicle´s aerodynamic characteristics can be changed by altering the angle of the wings. This alteration will result in a different projected area and lift coefficient. The values found in the table are according to the measurements taken before the disassembly of the formula student.

3.2.1. Aerodynamic Forces

Aerodynamic forces relate with the vehicle´s air contact. Meaning that the force magnitude increases with the vehicle speed. The aerodynamic forces can be divided in 2 categories (Figure 3.3):

1. Downforce
2. Air resistance (Drag)

Downforce is caused by the front and rear wing of the vehicle pushing it to the road while traveling at speed. This force is related with the projected area of the wing. On the other hand, air resistance is caused by the vehicle trying to move through the air. According to K. Rao, "Drag is a force acting opposite to the relative motion of any object moving with respect to a surrounding fluid" [21].

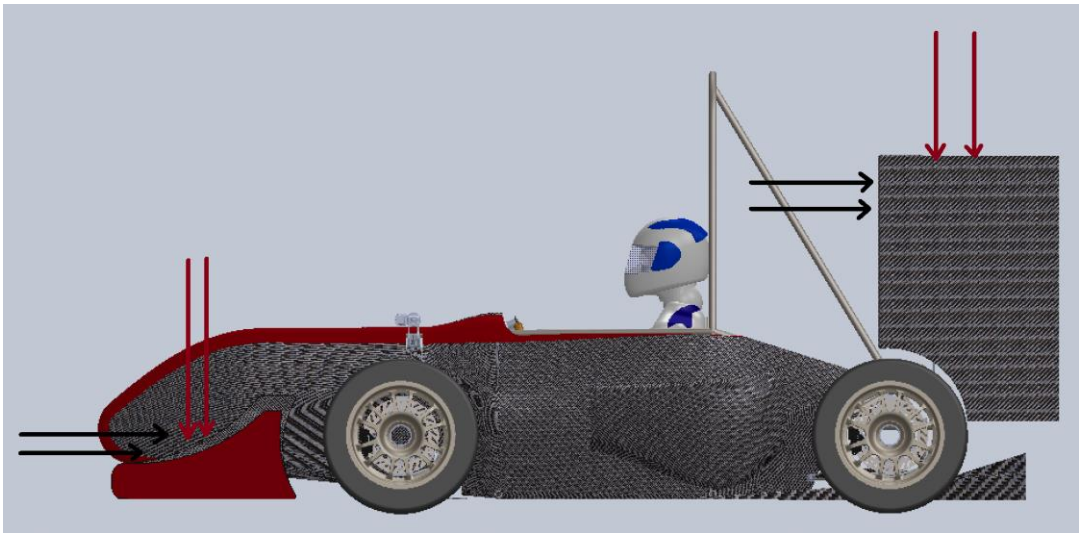

Figure 3.3- Representation of drag and downforce.

The downforce applied to the system can be calculated according to equation 3.1. The equation relates air density (ρ), lift coefficient (C_l), projected area of the wing (A_w) and vehicle speed (v). The reference area found in downforce and drag equations (A) is often the orthographic projection of the object (frontal area) on a plane perpendicular to the motion direction.

$$F_d = \frac{1}{2}.\rho.C_l.A_w.v^2 \quad \textbf{(3.1)}$$

It is important to notice that velocity has a quadratic influence in the equation result. Since air density, projected area and lift coefficient are constant, velocity will impact drastically the equation result. Above all it is important to understand this relation. Wings are set at a certain angle dictating the amount of air flowing above them. However, if the car is moving slowly there would not be enough air passing by the wings to provide downforce. On the other hand, if the car is moving at high speeds there will be more air passing by the wings, hence providing more downforce.

The downforce application point on the vehicle is according the wing projected area. Meaning that the downforce application point on each wing must be transferred to the vehicle according wing location (See figure 3.4 and 3.5).

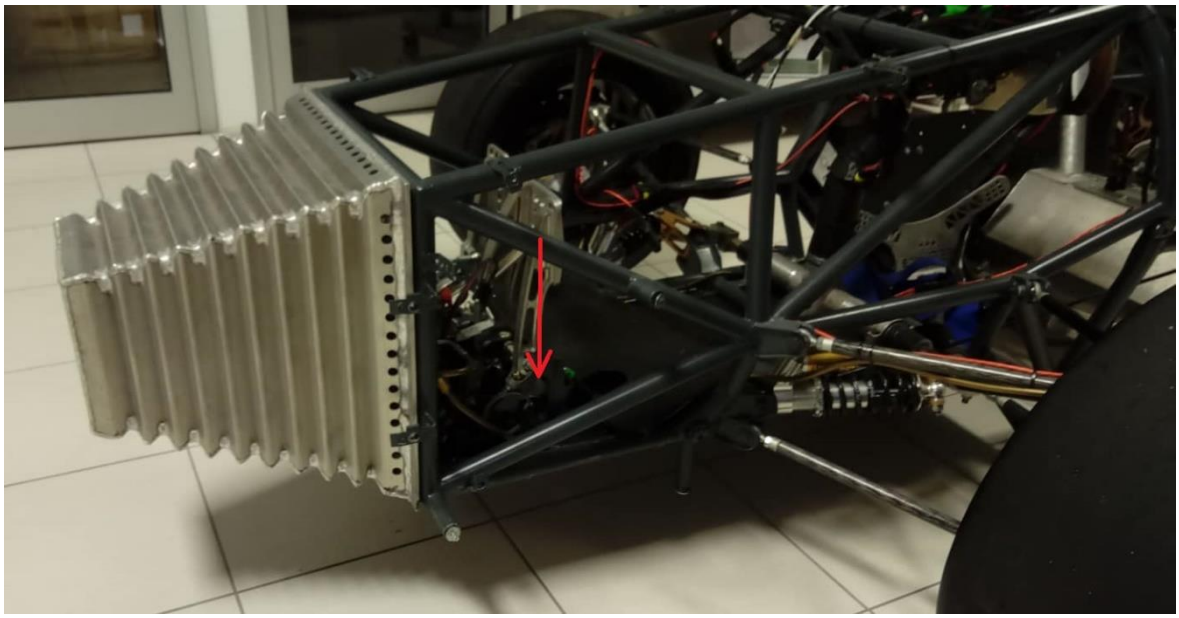

Figure 3.4- Front wing attachment points.

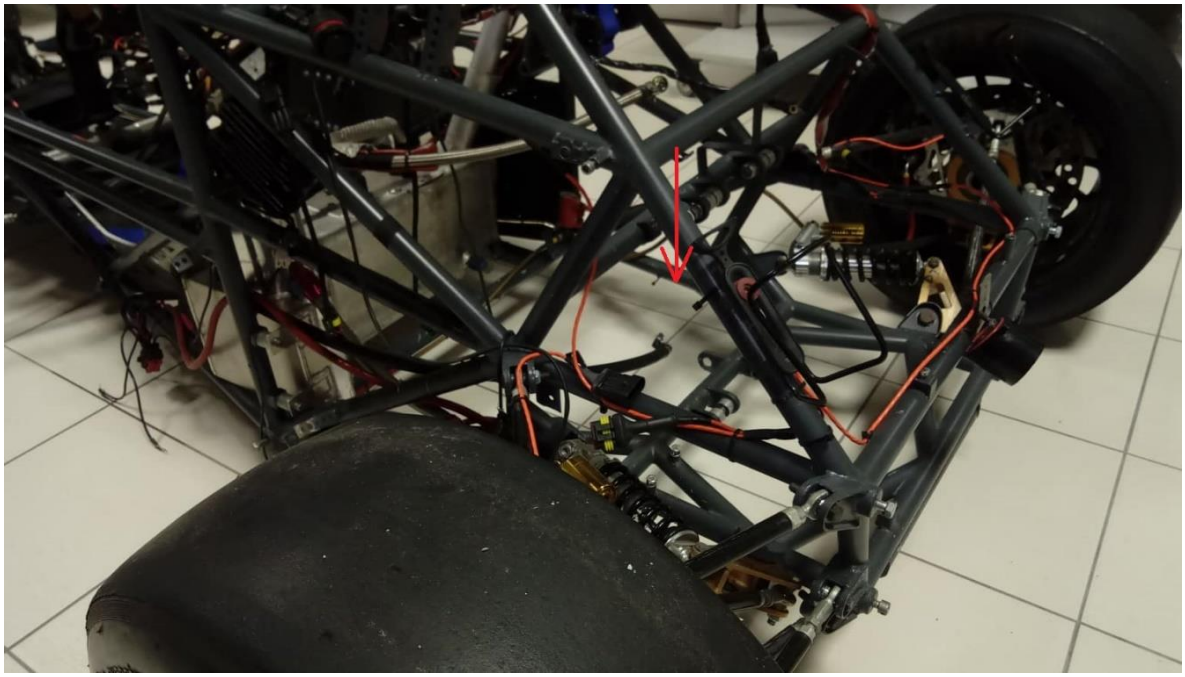

Figure 3.5- Rear wing attachment points.

According to the wing projected area, the downforce application points on the vehicle will be around the wing connection points. The exact location of the downforce application points will be presented in the following chapter.

Drag, also known as air resistance, similarly to downforce, relates velocity (v) and air density (ρ). The other variable is the projected area of the front of the single seater (A_f) and drag coefficient (C_d). The relation between the variables is the same as in equation 3.1. as shown in equation 3.2.

$$F_{drag} = \frac{1}{2}.\rho.C_d.A_f.v^2 \quad (3.2)$$

Once more, velocity is the main factor influencing drag. In a real-life scenario, it becomes more difficult to overcome the air barrier with the speed increase.

According to Formula Student Data, the single seater will not overcome 100 km/h so it is important to know how this speed will affect the forces imposed to the system. Considering the data from table 3.1, and considering a 100 km/h road speed, it was possible to calculate the aerodynamic forces, as presented in table 3.2.

Table 3.2- Results from Maple Software regarding aerodynamic forces.

Variable	Value (unit)
Downforce at the front	75.62 N
Downforce at the rear	75.62 N
Drag force	340.28 N

It is now possible to have a better understanding of the magnitude of the forces acting on the vehicle while traveling at 100 km/h. The downforce would be of 75.62 N at the front and back, a total of 151.24 N. Since the single seater weights 3531.6 N with a driver, the total downforce applied to the system corresponds to a 4.3 % weight increase (equation 3.3).

$$W_{gain} = \left(\frac{151.2}{3531.6}\right).100 = 4.3\ \% \quad (3.3)$$

In normal conditions the force provided by the wings does not translate in a big dynamic improvement. In low speed cases the downforce increase can be dismissed. Nevertheless, it cannot be forgotten that the angle and size of the wings can be changed, thus changing the magnitude of the force.

Regarding air resistance it acts as a barrier to speed increase, at 100 km/h the force acting with opposite direction to the movement of the car is of 340.28 N. This value, similarly, to downforce, grows with speed increase. As a reference, the value of drag at a speed of 50 km/h would be of 85 N.

In conclusion both aerodynamic drag and downforce play a role in slowing a vehicle down. Downforce allows for the vehicle to grip to the surface when in braking conditions it starts to slide, even if by just adding 147.15 kg to the car´s mass. On the other hand, air resistance imposes a force with opposite direction of the motion of the car that contradicts the single seater´s movement.

3.2.2. Load transfer

There are two main types of load transfer, lateral load transfer and longitudinal load transfer. The main goal during this section is to understand load transfers and how they affect

handling during braking conditions. Both lateral and longitudinal loads depend on the vehicle mass centre [22].

Lateral load transfer occurs during cornering. It can be defined as the shift of mass across the wheels due to lateral acceleration and centrifugal force.

While cornering a vehicle creates a force known as centrifugal force that acts against the lateral acceleration which is created by the grip from the tyres (See figure 3.6).

Figure 3.6: Lateral forces during cornering. Adapted from [22]

It is possible to relate lateral acceleration (Ay) and centrifugal force while cornering. Centrifugal force always acts in the opposite direction of lateral acceleration and will be the product of vehicle mass (W) and acceleration as shown in equation 3.4 [22].

$$Centrifugal\ Force = -W.A_y \tag{3.4}$$

Longitudinal load transfer occurs during acceleration or braking when a reaction force is generated. For example, during acceleration, a force with opposite direction of the vehicle´s movement will occur until the vehicle reaches a constant speed.

Both longitudinal and lateral load transfer are important factors that need to be considered when studying vehicle dynamics. For the purpose of the present project the main attention will be for longitudinal load transfer occurring during braking manoeuvres.

For the present study, the considerations taken were the following:

- The vehicle brakes in a straight line
- The mass centre is located at equal distance from left and right wheels
- The 4 tyres are in constant contact with the ground

Since the different types of load transfers are already defined, it is imperative to find the point in which the load will be applied to continue with calculations. See image 3.7.

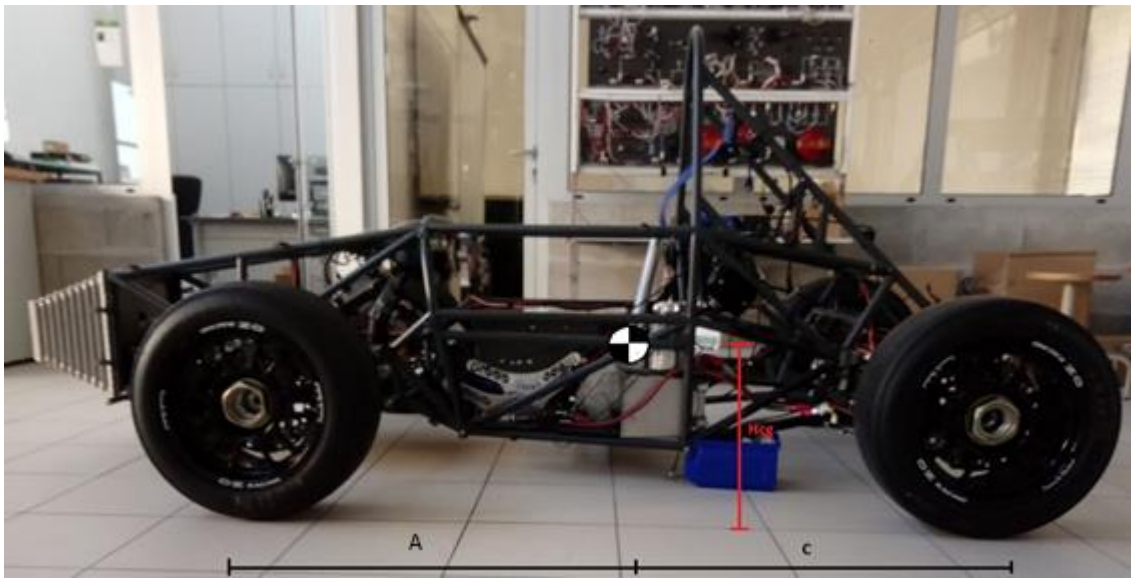

Figure 3.7- Striped vehicle main dimensions.

Analogous to what was explained before, during a braking maneuverer the vehicle rolls forwards. Meaning that the front wheels will be under more stress than the back wheels. Consequently, the front brakes will withstand most of the forces applied to stop or slower the vehicle down. So, the front brakes will be the reference for studying the system. It is obvious that if the front brakes can impose and withstand the forces needed to stop the car, so will the back brakes.

3.2.3. Resultant Forces

At this point of the study the main goal is to find the forces acting on the tires during a braking maneuverer. Tires are the only part of the vehicle in direct contact with the ground. There is no point in applying a tremendous amount of force on the brakes if the tyres can not deal with the deceleration imposed, therefore locking, and making the vehicle slide. So, to calculate the resultant forces acting on the tyres the variables presented in table 3.3 were considered.

Table 3.3- Variables to calculate tyre resultant force.

Variable	Value (unit)
Drag force	340.28 N
Front wing's downforce	75.62 N
Rear wing's downforce	75.62 N
Vehicle's mass (with pilot)	360 kg
Gravity acceleration	9.81 m/s^2
L1	510 mm
L2	833.86 mm
L3	760.14 mm
H1	219.80 mm

In the free body diagram presented in figure 3.8 all the forces acting on the vehicle during a braking manoeuvre are considered, allowing the definition of the balance equations (3.5, 3.6 and 3.7).

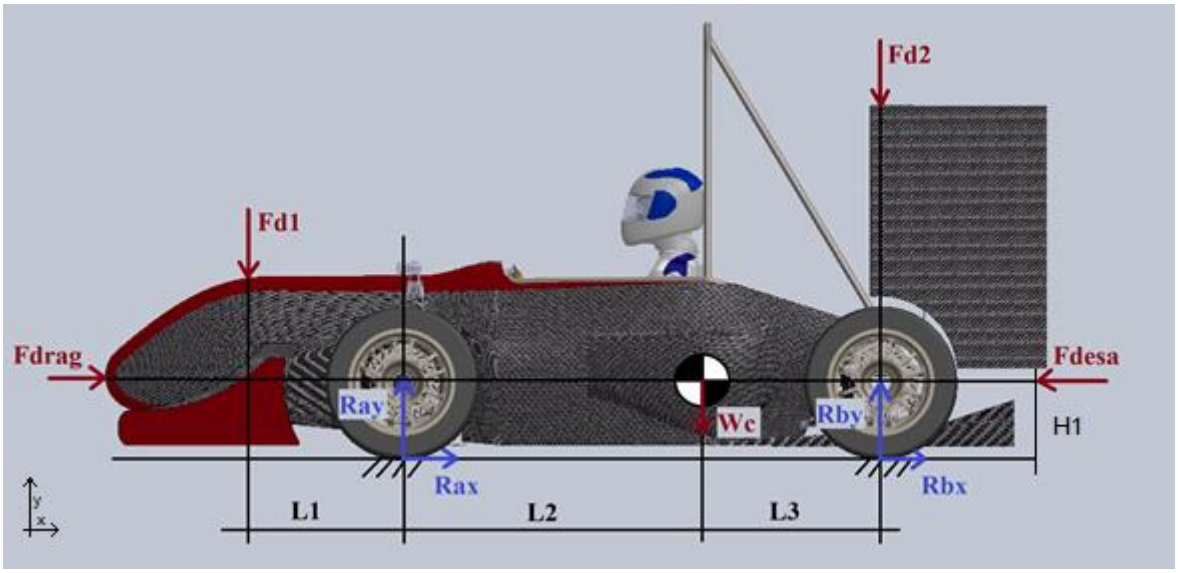

Figure 3.8- Forces acting on the single seater.

The balance equations for the static system presented are as follows:

$$\sum F_x = 0 \rightarrow F_{ar} + R_{ax} + R_{bx} - F_{dec} = 0 \quad (3.5)$$

$$\sum F_y = 0 \rightarrow -F_{d1} + R_{ay} - W_c + R_{by} - F_{d2} = 0 \quad (3.6)$$

$$\sum M_a = 0 \rightarrow L_1.F_{d1} - H_1.F_{ar} - L_2.W_c + (L_2 + L_3).R_{by} + H_1.F_{dec} - (L_2 + L_3 + L_4).F_{d2} = 0 \quad (3.7)$$

R_a and R_b represent the tyres reaction with the road. For each of the tyres the resultant force can be divided in 2 vectors, a horizontal and a vertical one. These vectors are related in the matter that one is equal to the other when multiplied by the friction coefficient (See equations 3.8 and 3.9).

$$R_{ax} = R_{ay}.\mu \quad (3.8)$$

$$R_{bx} = R_{by}.\mu \quad (3.9)$$

Coefficient of friction measures the amount of friction between two surfaces. A high value indicates that the force required for sliding to occur is higher than the force required when the coefficient is low. Friction coefficient between the asphalt and the rubber tyres is of 1.3 considering a dry surface and regulated tyres, according to AVON tyres motorsport [23].

Deceleration force is caused by vehicle braking and its units are g, with the gravitational acceleration of 9.81 m/s^2. So, deceleration force in becomes as shown in equation 3.10.

$$F_{dec}(g) = \frac{F_{dec}}{m.g} \quad (3.10)$$

Considering the system balance equations (equations 3.5, 3.6 and 3.7), the relation between tyre forces and friction coefficient (equations 3.8 and 3.9) and deceleration force (equation 3.10) it is possible to find the resultant forces acting on the tyres during braking.

The results obtained are shown in table 3.4.

Table 3.4- Resultant forces acting on each pair of tyres.

Variable	Value (unit)
Front tyre vertical reaction (axle)	2446.03 N
Front tyre horizontal reaction (axle)	3179.84 N
Rear tyre vertical reaction (axle)	1236.81 N
Rear tyre horizontal reaction (axle)	1607.85 N

The values of R_{ax} and R_{bx} are 3179.84 N and 1607.85 N, respectively. Deceleration causes the horizontal component of the tyres reaction force to be greater than the vertical component. It is also the reason why R_{ax} is higher than R_{bx}. During a braking manoeuvre, the vehicle rolls forwards due to the deceleration force acting on the gravity centre, causing the front wheels to be under more stress than the back ones.

As shown in figure 3.8, only two wheels were considered (axle), so R_a and R_b values correspond to both front and rear wheels respectively. In table 3.5, the resultant horizontal forces acting on each tyre are presented.

Table 3.5- Resultant forces acting on each tyre.

Variable	Value (unit)
Front right tyre horizontal reaction	1589.92 N
Front left tyre horizontal reaction	1589.92 N
Rear right tyre horizontal reaction	803.92 N
Rear left tyre horizontal reaction	803.92 N

The value in which further calculations will be based on is the front wheel horizontal reaction force. Different side wheels from the same axle have the same reaction forces. The value to consider is 1589.92 N.

3.2.4. Brake Torque

During a braking maneuverer, while the driver presses the brake pedal, the brake pads are pushed against the disc creating friction, thus stopping the vehicle.

Brake torque allows for the determination of maximum pressure that can be applied to the brake disc without wheel slide occurring. To continue with calculations, the rolling radius needs to be determined. The vehicle is equipped with 13-inch O.Z. alloy wheels and AVON tyres in all 4 corners, as shown in table 3.6 [23].

Table 3.6- Formula student tire size. Adapted from [23]

TYRE SIZE	RIM CHOICE	RIM USED	MEASURED AT		DIAMETER		SECTION		TREAD		REVOLUTIONS		TREAD PATTERNS
			PSI	BAR	INS	MM	INS	MM	INS	MM	MILES	KM	
6.0/19.5-13	5.5 - 6.5	6.00	20	1.36	19.35	491	6.60	168	6.10	154	1042	651	VIEW
6.5/19.5-13	5.5 - 7.0	6.00	20	1.36	19.25	488	6.80	173	6.30	160	1048	655	VIEW
7.0/19.5-13	5.5 - 8.0	6.00	20	1.36	19.30	490	7.10	180	6.90	175	1045	653	VIEW
7.0/20.0-13	6.0 - 8.0	7.00	20	1.36	20.10	510	8.00	203	7.40	187	1003	627	VIEW
7.2/20.0-13	6.0 - 8.0	8.00	20	1.36	20.20	513	9.00	229	7.10	180	998	624	VIEW
7.5/20.0-13	6.5 - 8.5	8.00	20	1.36	20.25	514	9.00	229	7.70	195	996	622	VIEW
8.2/20.0-13	7.0 - 9.0	9.00	20	1.36	19.95	506	9.75	248	8.50	215	1011	632	VIEW

Knowing the tyre dimensions, it is possible to calculate the maximum brake torque by multiplying the tyre rolling radius (R_{wh}) by the horizontal tyre reaction (R_{ax}), as shown in figure 3.9.

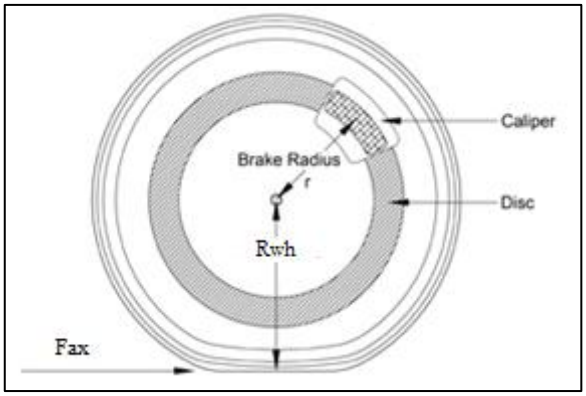

Figure 3.9- Rolling tyre dimension. Adapted from [24]

Since tyre diameter is known, it is now possible to determine maximum brake torque according to equation 3.11.

$$T_f = R_{ax}.R_{wh} \tag{3.11}$$

Maximum brake torque will occur in the front wheels as explained in 1.3. T_f stands for the maximum brake torque at each front wheel and has a magnitude of 407.81 N.m.

During races, for different road conditions a different type of tyre can be used, thus changing rolling radius (R_{wh}) and friction coefficient (μ).

3.2.5. Hydraulic Brake Pressure

To stop the vehicle, brake pads are pushed against the disc brake as explained before, imposing a force (F) perpendicular to the rotor plane. The pressure created by the cylinders is calculated by dividing the force (F) by the cylinder contact area (A), as represented in Equation 3.12.

$$p = \frac{F}{A} \tag{3.12}$$

Each calliper contains 2 cylinders, on different sides of the calliper, opposed to each other as shown in figure 3.10.

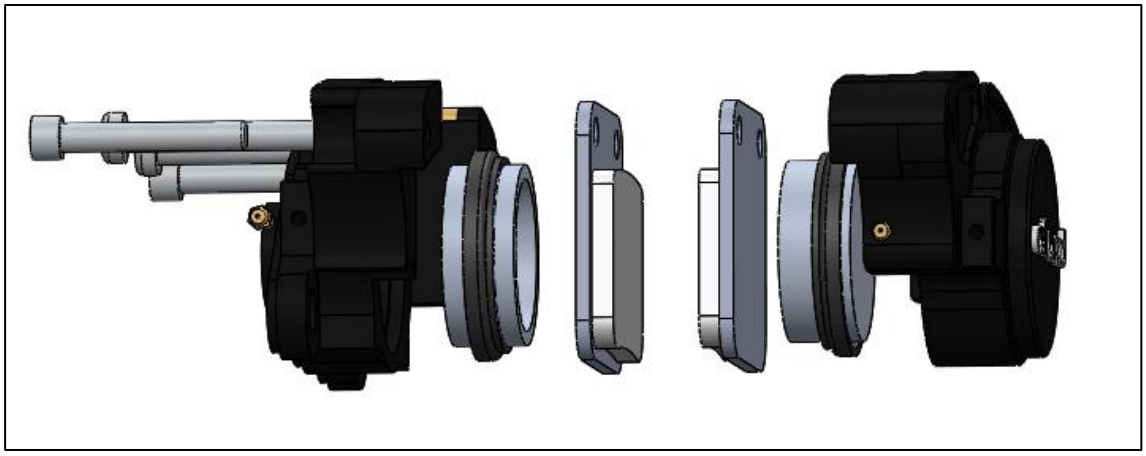

Figure 3.10- Calliper exploded view.

At this point, one of the brake callipers already installed in the single seater was disassembled to get more accurate measures regarding cylinder size. Once disassembled the cylinder's diameter (D_{cyl}) was measured at 31.75 mm. Therefore, the area actuated in each wheel by the brake calliper (Acyl) will be of 0.00158 m^2, according to equation 3.13.

$$A_{cyl} = \pi . (\frac{D_{cyl}}{2})^2 . 2 \tag{3.13}$$

Inside the wheel hub, both cylinders actuate the brake disc at the same place, but at different sides. It was assumed the pressure centre at 2/3 of outer radius of the rubbing path of the disc and thus the friction drag force also acts on the disc at this radius, which is termed the "effective radius" (R_{ef}), to generated braking torque, with the equation 3.14 from [25].

$$R_{ef} = R_i + \frac{2}{3}.(R_e - R_i) \quad \textbf{(3.14)}$$

Nominal pressure between the brake pad and the disc during braking is usually between 1 and 10 MPa. The true contact area however is a proportion of the total pad area, 20% to 60% for moderate braking loads, distributed over several small areas (plateaux) that protrude by a few microns above pad surface. This factor is mainly related with brake pad material and fabrication methods and will influence pad behaviour during braking.

Brake pad friction coefficient affects vehicle performance during braking in the way that neither a too high nor a too low value is good. If friction coefficient is too low, brake will not be flexible. If the coefficient is too high wheel lock will occur. According to European standards brake pads are best suited to work in a high temperature environment of 100 to 300 ºC [26].

A brake pad friction coefficient of 0.56 was considered, according to European standards. Considering all variables, it was possible to calculate maximum pressure (P_{hmax}) that can be imposed to the callipers without wheel slide occurring, according to equation 3.15.

$$P_{hmax} = \frac{T_f}{\mu . A_{cyl} . R_{ef}} \quad \textbf{(3.15)}$$

The value for maximum hydraulic brake pressure on the calliper without occurring wheel slide is of 44.65 bar. Meaning that during a brake manoeuvre, in dry asphalt, using the tyres indicated in table 3.6, the force imposed by the driver on the brake pedal should never be more than the enough to produce 44.65 bar of hydraulic pressure on the calliper. Otherwise, tyre lock will occur, and the vehicle will slide.

3.2.6. Maximum Friction Force

Maximum brake friction force (F_{fri}) is the maximum force applied to the calliper by the disc during braking considering the maximum brake torque. F_{fri} is perpendicular to the slave cylinders movement plane and coplanar to R_{ax}, as represented in figure 3.11.

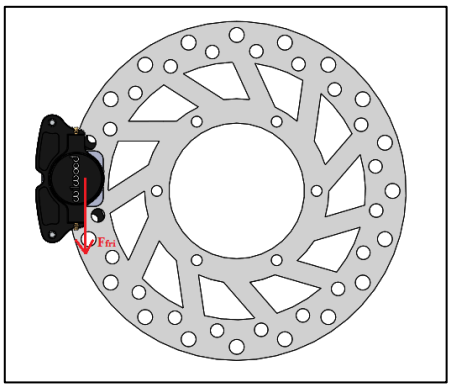

Figure 3.11- Friction force representation. Adapted from SW.

To obtain the maximum force acting on the calliper, maximum brake torque (T_f) must be divided by the disc's effective radius (R_{ef}). See equation 3.16.

$$F_{cmax} = \frac{T_f}{R_{ef}} \tag{3.16}$$

The maximum frictional force (F_{cmax}) acting on the callipers is of 3959.36 N. In each brake pad acts ½ of F_{cmax} since there is a couple for each calliper.

3.3. 2nd Approach

The second approach consists in the brake system study considering the maximum force applied by the driver on the brake pedal. Until this point all calculations took in account the maximum brake force that could be applied without wheel lock occurring. However, in some scenarios, it is possible for the driver to apply a force on the brake pedal higher than the force needed to lock up the wheels. Therefore, if the system is designed taking only in consideration the 1st scenario, the possibility for brake failure increases.

At this point the maximum force that can be applied by the driver on the brake pedal regarding wheel lock is considered. The force will be transmitted to the master cylinder through the brake pedal. Depending on master cylinder characteristics the force imposed will translate in fluid pressure that will feed the calliper´s cylinders, pressing the brake pads against the disc.

First and foremost, it is important to understand the forces applied to the pedal system that are represented in figure 3.12.

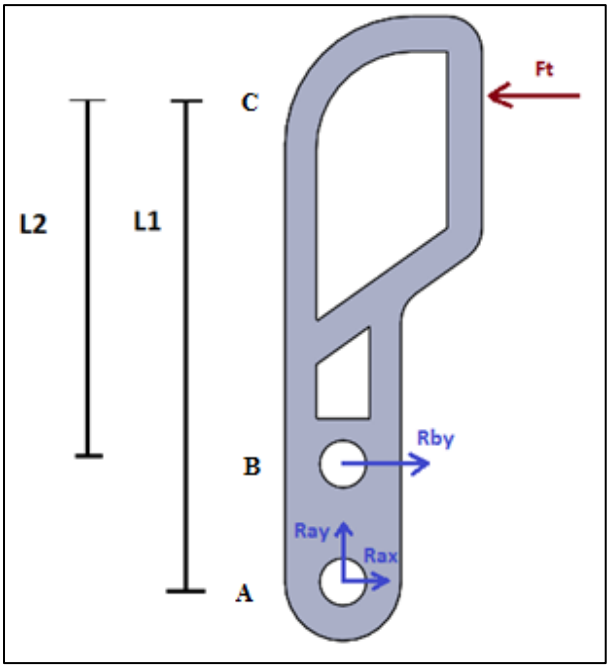

Figure 3.12- Brake pedal representation.

During braking, when the driver pushes the pedal forward, a force F_t is applied in C. The brake pedal is attached to the vehicle on point A and to the master cylinder on B. So, when the force is applied to the pedal, it will rotate over its support point A. The force transmitted to the master cylinder will depend on the actual force applied by the driver and the dimensions L1 and L2.

For this approach it is important to consider a "panic scenario", meaning that the driver will impose to the pedal a force quite superior to the one needed to stop the vehicle without wheel slide occurring.

According to formula student regulations, the pedal box assembly should be able to support a force of 2 kN without any damage occurring in the box or in adjacent systems [27]. Therefore, the maximum force to consider on the brake pedal is 2000 N.

3.3.1. Force Applied to Master Cylinder

The human body is a complex machine capable of producing great strength that translates in great forces. Strength is the ability to generate muscular tension and to apply it to an external object through the skeletal lever system. Sheer muscle mass (thus, body size) is a significant factor, with cross-sectional area of the muscle fibbers being a major determinant of the maximum force that can be generated. Maximum muscular force (strength) can be exerted for only a few seconds [28].

For the present study, the forces will be imposed by the driver leg which activate the brake pedal. Legs possess the biggest muscles in human body, thus capable of imposing forces of great magnitude.

As explained before (section 3.3), the single seater pedal box must be able to withstand a maximum force of 2000 N without suffering any damage in the structure or sub adjacent systems. So, to obtain a correct study of the brake system, a maximum force of 2000 N was considered as the maximum force to be applied on the brake pedal (F_t).

Equations 3.17, 3.18 and 3.19 allow the determination of the force imposed to the master pump.

$$\sum F_x = 0 \rightarrow R_{bx} - F_t + R_{ax} = 0 \quad \textbf{(3.17)}$$

$$\sum F_y = 0 \rightarrow R_{ay} = 0 \quad \textbf{(3.18)}$$

$$\sum M_a = 0 \rightarrow F_t * L_1 - R_{bx}.L_2 = 0 \quad \textbf{(3.19)}$$

The brake pedal dimensions are presented in table 3.7.

Table 3.7- Brake pedal system variables.

Variable	Value (unit)
Force applied to the brake pedal	2000 N
L1	240 mm
L2	165 mm

The resultant force acting on the master cylinder has a value of 6400 N, according calculations.

The vehicle in question has 2 central master cylinders, as required by regulations. One for both the front wheels and one for both the rear wheels. Since there are 2 master pumps and no brake limiter, a mechanism of force distribution is required. Otherwise the force imposed on the pedal would result in equal pressure on all 4 callipers. The mechanism used to regulate force distribution on the master cylinders is shown in figure 3.13. It allows the distance between the force application point on the pedal, and the master pumps to be changed, therefore changing the amount of force applied in each pump. If the master brake cylinders are equidistant from the force application point, the force applied on each one will be half of Rbx.

The force imposed to the front wheels master cylinder must be greater than the one imposed to the rear ones. During a braking manoeuvre, the vehicle rolls forward due to weight transfer towards the front. Therefore, the front brakes can create more pressure on the disc without wheel slide occurring. To proceed with calculations, a maximum distribution of 80 % of brake force was considered. It means that the regulation mechanism allows a maximum of 80 % of brake force to be applied on the front brakes master pump, as shown in equation 3.20.

$$F_{mc1} = 0.8.Rbx \tag{3.20}$$

Considering an 80% force distribution, 5120 N are applied to the front brakes master cylinder, while the remaining 20 % are applied to the back brakes' master cylinder.

In a real-life scenario, the maximum force applied to the brake pedal would be when the driver experiences a "panic situation", meaning that the brake pedal would be pushed with the driver maximum force.

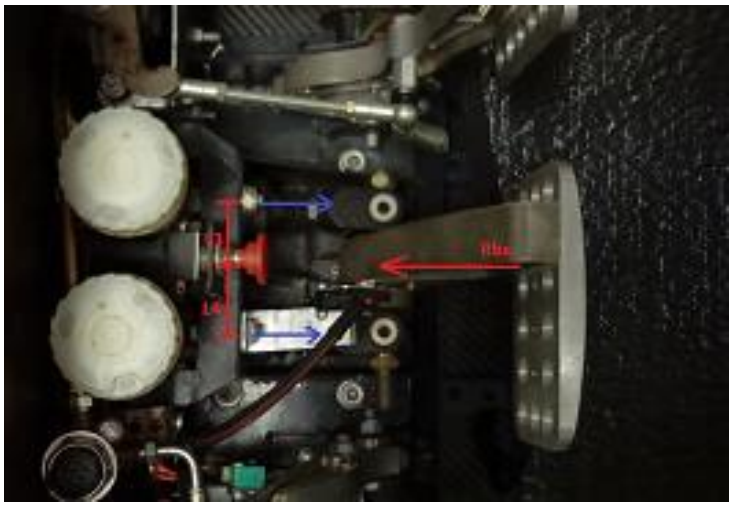

Figure 3.13- Brake partition system.

3.3.2. Master Cylinder Characteristics

Master cylinder is a control device that converts force into hydraulic pressure. The force is imposed by the driver when pressing the braking pedal. Pedal movement forces the dislocation of a cylinder along master's cylinder bore, this movement is transferred through hydraulic fluid resulting in slave cylinder movement. Two AP Racing (CP2623-88) master cylinders were chosen following the dimensions presented in figure 3.14 [29].

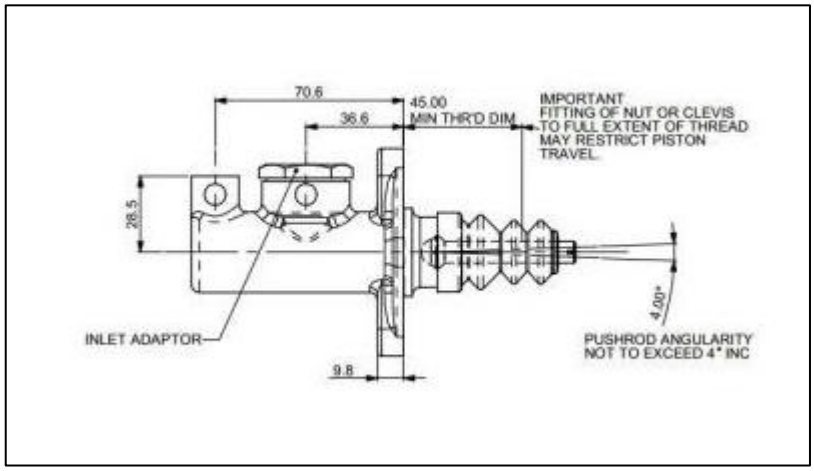

Figure 3.14- Brake Master Cylinder. Adapted from [29]

Hydraulic pressure created by the movement of the piston inside the master cylinder compresses the fluid evenly, but by varying the area of the cylinder the force can be changed. When the forward movement of the pistons causes their primary cups to cover the bypass holes, hydraulic pressure builds up and is transmitted to the wheel cylinders. When the brake pedal retracts, the pistons allow fluid from the reservoir(s) to refill the chamber if needed.

According to AP Racing official website the inside dimensions of the master cylinder are as presented in table 3.8 [29].

Table 3.8: Master pump internal dimensions.

Variable	Value (unit)
Bore	23.80 mm
Push rod length	115 mm
Full stroke	25.40 mm
Travel to cut-off	0.68 to 1.09 mm

Knowing the characteristics of the master brake pumps it is possible do calculate maximum hydraulic pressure in the system, through the equation 3.21.

$$P_{hid} = \frac{F_{mc1}}{A_{cyl}} \tag{3.21}$$

F_{mc1} refers to the force applied to the master pump, presented in equation 3.20. While A_{cyl} refers to the master cylinder area inside the brake pump. The maximum hydraulic pressure applied to the system, according equation 3.21, is of 115 bar.

3.4. Conclusions

Formula student brake system study presented until this point was important to establish the forces and constrains to be considered during component optimization. From the 1st approach it was possible to conclude that the maximum frictional force acting on the brake callipers without wheel slide occurring is of 3959.36 N, corresponding to a brake pressure of 44.65 bar.

The 1st approach study represents the most common brake scenario. When the driver imposes a brake pedal force superior to the one needed to produce 44.65 bar of pressure, the vehicle's front wheels lock and the pressure is immediately relieved to unlock them. The 2nd scenario study is representative of a panic scenario. The driver imposes a maximum force of 2 kN to the brake pedal generating a brake pressure of 115 bar. However, this situation will most likely never occur, nevertheless it must be considered, because it is stipulated in the regulations.

The 1st scenario will be the most prevalent during a competition where the driver will always be pushing the grip limits of the vehicle. For that reason, it is of extreme importance to consider a safety factor to 1st approach load conditions, regardless the 2nd scenario. A safety factor of 1.5 was imposed to the 1st scenario load conditions to ensure the safety of components design. Therefore, the new load conditions acting on each calliper for static analysis are presented in table 3.9.

Table 3.9- Load conditions for calliper static analysis.

	1st Scenario	2nd Scenario
F_{cmax} (N)	5940	5940
P_{hmax} (bar)	67	115

Each calliper is a two-part assembly, and each half contains a brake pad. Therefore, the force distribution is as shown in figure 3.15.

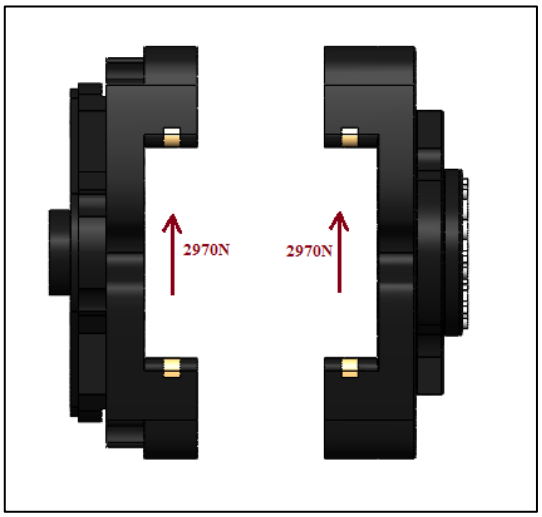

Figure 3.15- Frictional force on the calliper.

When the brake pedal is pressed hydraulic pressure is imposed to all the brake system, from the master cylinder to the front slave cylinders. Inside the callipers the cylinders are pushed against the disc leading to a reaction on the callipers with the same magnitude as the pressure imposed to the system. Hydraulic pressure pushes the callipers apart as shown in figure 3.16.

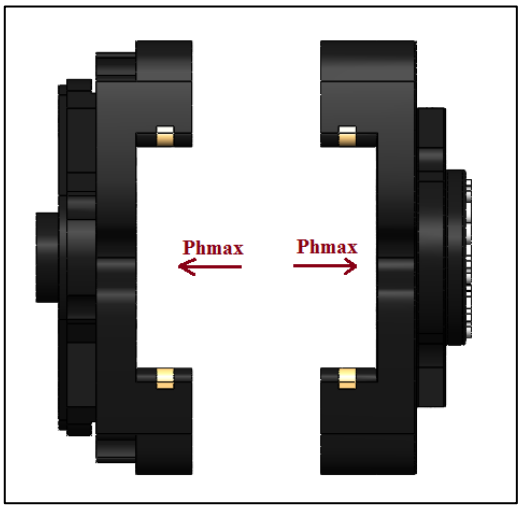

Figure 3.16- Hydraulic pressure acting on the calliper.

Maximum tangential force observed, considering the 1.5 safety factor is of 2970 N in each half of each calliper. This is the maximum value of tangential force regardless of brake pressure, due to the friction coefficient between the tires and the road.

4. Standard Component

As mentioned before, the calliper used in the formula student vehicle is an off the shelf product from Wilwood. The calliper was produced using a high-quality aluminium alloy making it light and durable. The component is destined to be used in motorcycles or low-capacity engine vehicles, improving the brake system by reducing weight and increasing stopping power.

During the following sections the brake calliper will be analysed to understand its limitations and possible improvements. The forces acting on the system were determined during chapter 3 and represent the limit scenarios to which the component will be subjected.

4.1. 3D Modelling

To study the original component a CAD model was required. The SolidWorks computer software was used to design and study the component.

After all the measures were completed, the component was designed. It is important to notice that the main calliper structure can be divided in 2 parts. Both parts are connected using 2 M8 bolts. Only one of the parts is attached to the sleeve, allowing for the calliper to stay in place while the vehicle is moving (figure 4.1).

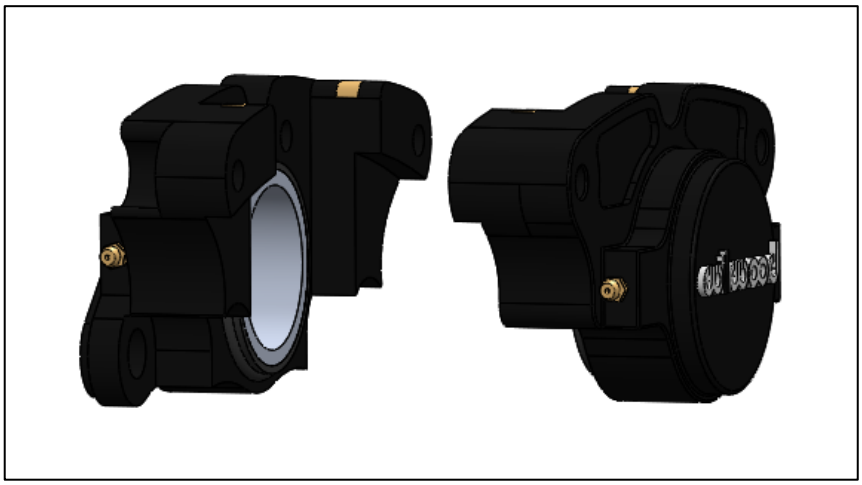

Figure 4.1- Brake calliper assembly. Adapted from SW.

Regarding component material, Wilwood does not specify the aluminium alloy type used to manufacture the brake calliper. However, according to Àdam Horváth *et al*, in "Development of brake calliper for rally-car", in the development of a similar type brake calliper, the material used to CNC manufacture the component was the 7075-T6 Aluminium Alloy, with the material properties according to table 4.1 [30].

Table 4.1- 7050-T73510 aluminium alloy properties

Property	Value	Units
Elastic Modulus	71999.9992	N/mm^2
Poisson's Ratio	0.33	N/A
Tensile Strength	570.0000034	N/mm^2
Yield Strength	505.0000031	N/mm^2
Tangent Modulus		N/mm^2
Thermal Expansion Coefficient	2.4e-05	/K
Mass Density	2810.000061	kg/m^3
Hardening Factor	0.85	N/A

The next step in component analysis is to simulate real life conditions using computer software, to understand component behaviour and possible improvements.

4.2. Static Study

The main goal of the static study is to understand the component behaviour during braking, analysing maximum stress and displacement occurred.

Calliper assembly is composed by 2 parts, part A and B, connected to each other by two M8 bolts, located on the part top sides (attachment points A1 and A2 for part A, B1 and B2 for part B). Part B is attached to the vehicle sleeve through two M8 bolts (attachment points B3 and B4).

While braking, hydraulic pressure is generated in the brake circuit pushing the slave cylinder against the brake pad, leading to a reaction force acting on the calliper with the same pressure. When pressing on the moving rotor, a tangential force acts on the pads and is transferred to the calliper through the slave cylinder. Both hydraulic pressure and tangential force are transferred to the cylinder case during a braking manoeuvre. This is transversal to both part A and part B. However, on part B also act the forces generated from part A. Meaning that for part B, not only tangential force and brake pressure must be considered, but also the reaction forces imposed by part A.

For the first part (part A), constrains were applied in the attachment points A1 and A2 preventing the component from moving. Regarding load application, both tangential force and pressure were applied inside the cylinder case, as represented in figure 4.2.

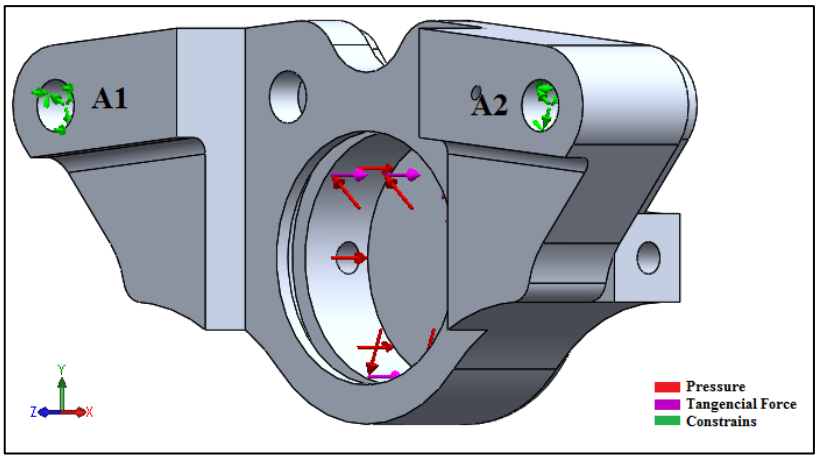

Figure 4.2- Part A loads and constrains.

For the second part (Part B), constrains were applied in the attachment points B3 and B4 connecting the calliper to the vehicle sleeve. Tangential force and pressure application points were the same as for part A (inside the cylinder case). It is important to also consider the loads imposed by part A acting on both attachment points B1 and B2, represented in figure 4.3.

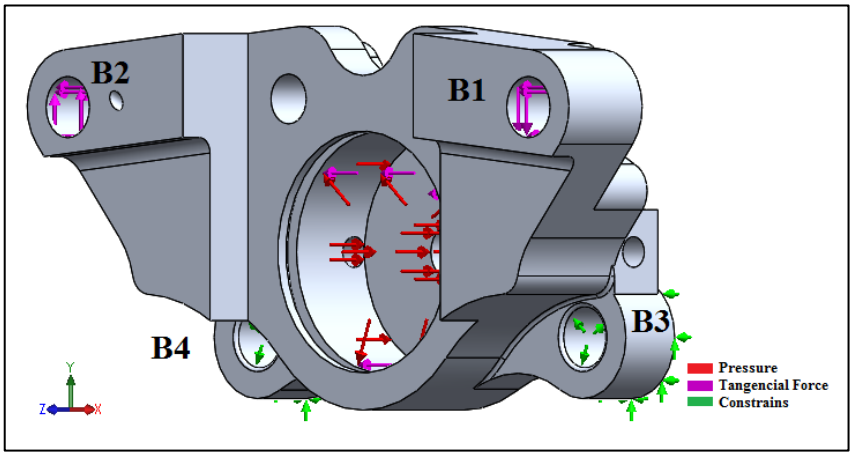

Figure 4.3- Part B loads and constrains.

According to chapter 3 the static study is divided in 2 scenarios:

Scenario 1: While braking, the maximum brake pressure for the vehicle to stop without wheel lock occurring is generated considering a safety factor of 1.5 (67 bar).

Scenario 2: While braking, in a panic situation, the driver imposes a force of 2 kN (the maximum force that the brake system must withstand without brake failure occurring, according to regulations) to the brake pedal, generating maximum brake pressure (115 bar) [27].

For both scenarios, the maximum tangential force of 5940 N considering a safety factor of 1.5 is considered, as referred in chapter 3.

4.2.1. Scenario 1

For the first part (part A) the loads and constrains were applied to the model. The pressure of 67 bar and the tangential force of 2970 N act on the slave´s cylinder sleeve. The hydraulic pressure pushes the calliper away from the rotor, while the tangential force pushes it in a direction tangential to the disc.

Once all variables were considered, it was possible to complete the static simulation. The software uses the maximum distortion criterion, also known as von Misses criterion, to evaluate the component´s stress. According to von Misses criterion, the maximum stress on the component is of 75.21 MPa and occurs in the area below the attachment points (A1 and A2). Maximum displacement on the component is of 0.074 mm along OZ axle, as represented in figure 4.3.

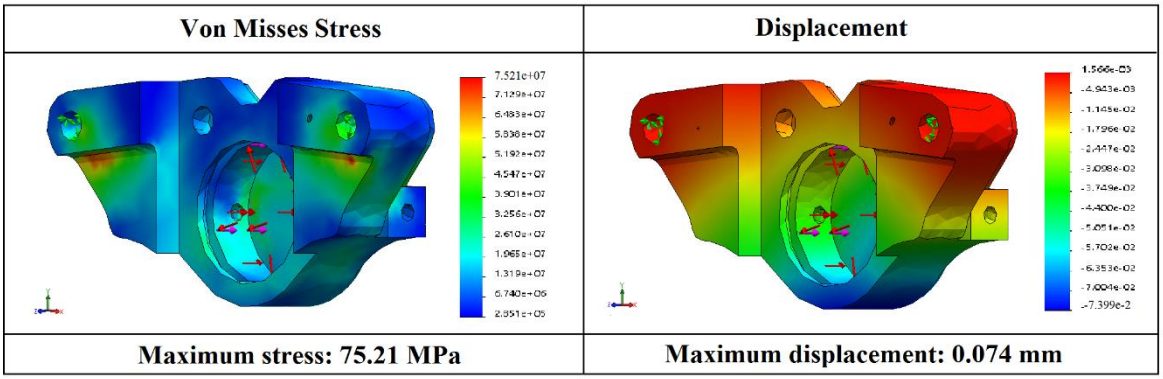

Figure 4.3- Part A, scenario 1, von Misses stress and displacement.

Maximum von Misses stress is lower than the maximum material yield stress, therefore, the component maintains its structural integrity when subjected to 67 bar of pressure and 2970 N of tangential force.

Similarly to what was done in part A, loads and constrains were applied to part B. However, it was necessary to consider, not only the 2970 N tangential force and 67 bar of pressure, but also the reaction forces from A1 and A2 to simulate the loads applied by part A.

After considering all variables it was possible to complete the simulation. According to von Misses criterion, the maximum stress observed in the component is of 357.90 MPa, taking place near the calliper to sleeve connection (B3 and B4). Maximum displacement occurs, once more in OZ axis, near the attachment point (B1), with a value of 0.20 mm (See Figure 4.4).

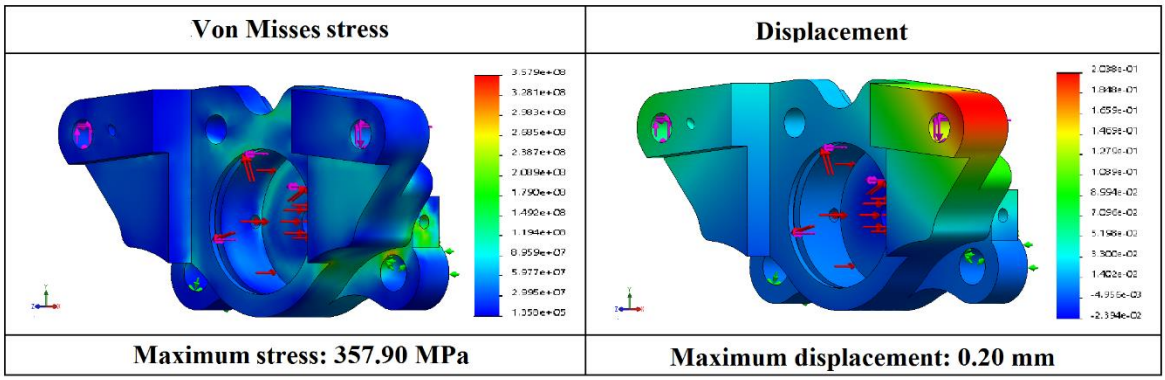

Figure 4.4- Part B, scenario 1, von Misses stress and displacement.

According to simulation results, it is possible to conclude that the original component withstands the loads applied during a regular brake manoeuvre. This study does not consider the panic scenario in which the maximum pressure is applied to the system, therefore it is imperative to proceed to scenario 2 analysis.

4.2.2. Scenario 2

In scenario 2 the maximum force applied to the brake pedal by the driver is considered. According to previous calculations (chapter 3), the force translates in a maximum pressure of 115 bar throughout the system.

Simulation procedure was the same as for scenario 1, apart from the pressure applied to the system (115 bar for scenario 2 and 67 bar for scenario 1).

For part A, according to von Misses criterion, the maximum stress is of 123.50 MPa, occurring bellow the attachment points. The maximum von Misses stress observed is below the maximum material yield stress of 505 MPa. Meaning that the component will withstand the load without plastically deform. Regarding maximum displacement, it occurs on the OZ axel with a maximum value of 0.13 mm in the cylinder cage lower region (See Figure 4.6).

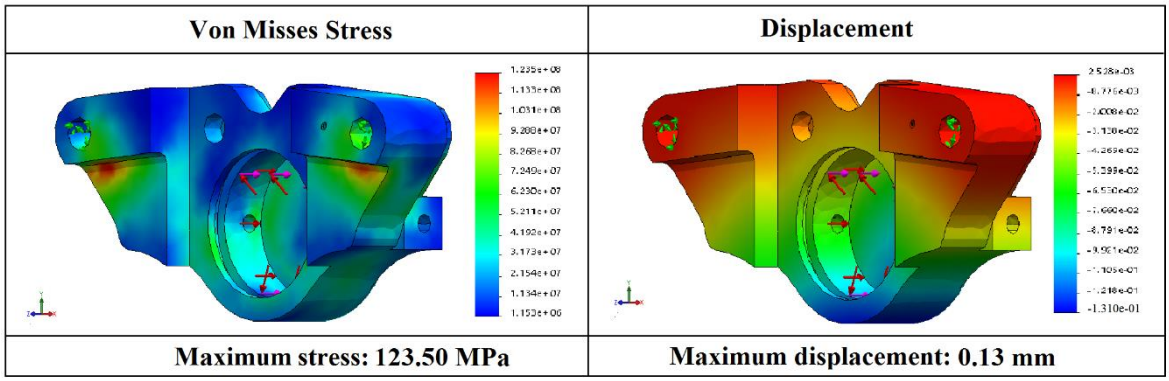

Figure 4.5- Part A, scenario 2, von Misses stress and displacement.

For part B, according to von Misses criterion, the maximum stress is of 495.10 MPa near the sleeve attachment points. This value is also inferior to the maximum material yield stress, meaning that the calliper withstands the load without braking. It is important to notice that maximum stress observed is near the material yield stress, which can be critical when considering a cyclic behaviour. Maximum displacement comes as 0.30 mm near B1 attachment point, shown in red in figure 4.6.

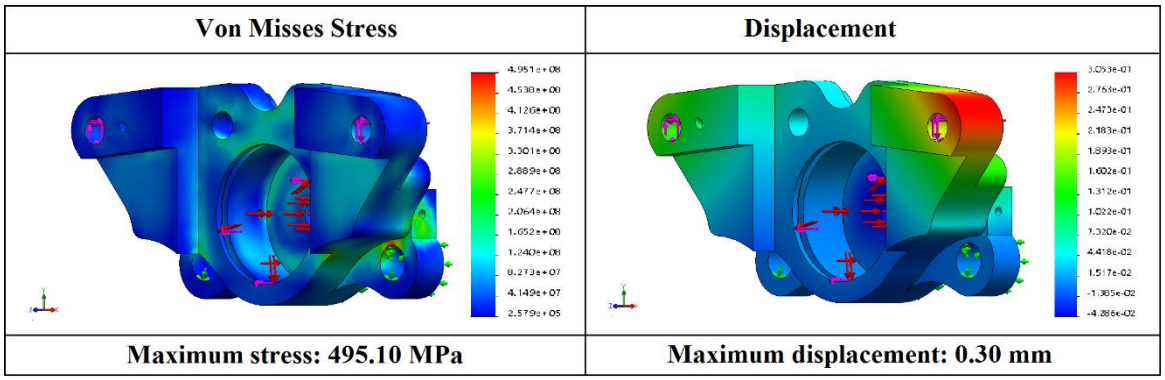

Figure 4.6- Part B, scenario 2, von Misses stress and displacement.

4.2.3. Conclusions

After completing simulation and analysis it is possible to conclude that the brake calliper can stand the loads imposed during a normal utilization (scenario 1). Maximum von Misses stress observed is below the maximum material yield stress with a safety factor of 0.7, considering the safety factor of 1.5 applied to the load conditions. Meaning that the component will not plastically deform or fracture during utilization.

In a limit situation (scenario 2) maximum von Misses stress observed is also bellow the material yield stress. Meaning once more, that the component will not plastically deform. However, it is important to mention that, in scenario 2, part B maximum von Misses stress is close to the material yield stress (505.00 MPa).

Regarding component displacement, in both scenarios, the maximum displacement observed is not sufficient to lead to system failure. The maximum displacement occurring during component utilization is not sufficient to limit piston travel. Therefore, the system is reliable and ready to deal with real life utilization conditions.

5. Prototype Stage

To produce a brake calliper with high mechanical properties with the intent of putting it to use in the new formula student vehicle, three prototypes were developed. Each prototype integrates a new design allowing for a reduction in weight and improvement in mechanical properties. The prototypes are based on a topologic study performed from the original calliper, following the steps presented in figure 5.1.

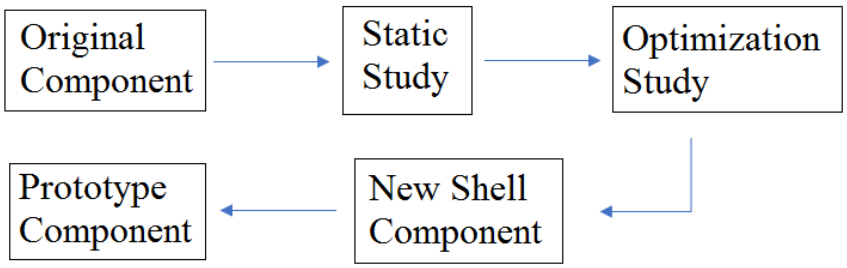

Figure 5.1- Steps to prototype design.

The original component is produced from a single block of high-grade aluminium alloy with high stiffness-to-weight ratio, making it very durable. However, it is possible to use another type of material as titanium to produce the new component, with better mechanical properties. Titanium is recognized for its high strength-to-weight ratio [31], reason for it to be chosen as the material for the new component. It is a material very hard to machine due to its stiffness and thermic characteristics (titanium does not dissipate heat through the part).

Each prototype design is based in an optimization study applied to the original component. This type of study allows for the determination of optimal component geometry based on material, goals and constrains set by the user. Optimization studies can be divided in two types:

1. Topology optimization: Removal of material in low stress areas based on loads and constrains applied to the component to minimize material usage in component production.
2. Generative design: Generation of a design that meets the requirements imposed by the designer (loads, constrains, dimensions and amount of material).

5.1. Optimization Study

To understand possible improvements in the original component geometry according to utilization conditions, a topological optimization study was conducted. This type of study allows material removal in low stress areas to reduce component mass.

To start the optimization study, it was important to select the base static study corresponding to the worst-case scenario: 115 bar of hydraulic pressure and 2970 N of tangential force applied (scenario 2).

The main objective was to create a component with same/better mechanical properties when compared to the original component. The titanium-alloy chosen for the new design was the Ti6Al4V titanium alloy with the characteristics presented in figure 5.2.

Chemical Composition (nominal) %

Element / Material	Ti	Al	V	Fe	C	N	O	H	Others	Total Others
Ti6Al4V (Gd 23) 20-63 µm	Bal.	5.50 - 6.50	3.50 - 4.50	0.25	0.08	0.03	0.13	0.0125	0.10	0.40

Chemistry according to F136, B348

Mechanical Data[1]	Formula Symbol and Unit	As-Built[2]	Heat Treated	+ HIP
Tensile strength	R_m [MPa]	1280	970	1000
Offset yield strength	$R_{p0,2}$ [MPa]	1135	880	895
Elongation at break	A [%]	8	14	15
Reduction of area	Z [%]	20	50	40
Young's modulus	E [GPa]	115	120	125
Vickers hardness	HV10	370	305	315
Impact energy	[J]	15	30	20
Roughness average	Ra [µm]	10	-	-
Mean roughness depth	Rz [µm]	70	-	-

Material Characteristics

- Good corrosion resistance
- High specific strength
- High cycle fatigue strength
- High toughness

Typical Application Areas

- Orthopedic implants
- Aerospace
- Automotive
- Energy applications

Figure 5.2- Ti6Al4V ELI mechanical characteristics. Adapted from [32]

When compared to 7050-T73510 aluminium alloy, Ti6AL4V ELI presents a higher value of yield and tensile stress. Meaning that by using this new material, it would be possible to obtain a component with the same rigidity as the original, using less material.

5.1.1. Topology study

For the topology study to be accurate, goals, constrains and manufacturer controls needed to be set up properly. These settings dictate study results and are the base for the optimization study. “Goals” define the study intent (best stiffness-to-weight ratio; minimum displacement; etc). “Constrains” define a limit to mass reduction (limit material removal by percentage). “Manufacturer controls” allows for the software to obtain a part that can be produced using a certain type of manufacture process (example: The software can create a part that is ready for CNC machine or mould casting without the need of redesigning the component).

To complete topology study, goals, constrains and manufacturer controls were defined as follows:

- Main Goal: Reduce mass material until best stiffness-to-weight ratio is achieved.
- Constrain 1: Do not remove more than 50% of material.
- Manufacturer control 1: Maintain 3mm of excess material near the attachment points.
- Manufacturer control 2: Maintain 2mm of excess material near cylinder case and pad support regions.

After running simulations using the SolidWorks computer software, a new optimized part was obtained, as shown in figure 5.3.

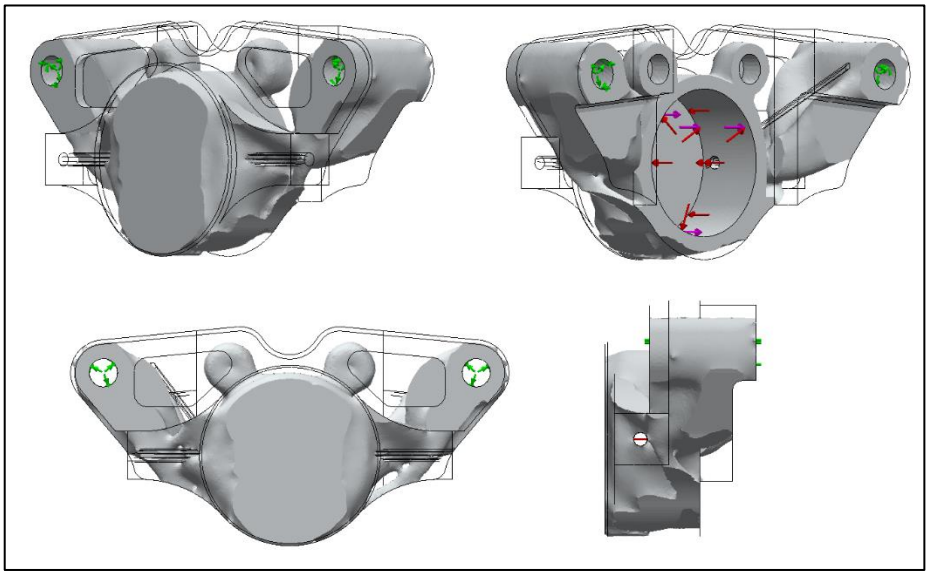

Figure 5.3- Topology study optimized part.

It is important to understand the results obtained to achieve the best design possible. The new part analysis, generated from topology study, considering the new material, allows for the following conclusions:

- There is a region between attachment points (A1; A2) and pad support structures where material can be removed.
- Walls connecting the cylinder case to the attachment points (A1; A2) can be redesigned using less material.
- Cylinder case wall thickness can be reduced.

5.1.2. Prototype Design

Prototype design is where, after analysing the data obtained from the topology study, a prototype is developed. It is possible to directly manufacture a component from topology study results due to Selective Laser Melting geometry freedom. However, it was chosen to redesign a new component based on the topology study results, instead of directly manufacture one.

According to optimization study results, it was possible to understand that the component main structural region was between the cylinder case and the attachment points (A1 and A2 for part A). Therefore, it would be possible to remove excess material around this region while maintaining the component structural integrity.

Before reaching a final design, three prototypes were designed. Each prototype integrated a different approach to reduce stress levels on critical points of the component based on the results of the topology study. It was known from the beginning that the original component

presented high stress values, in some regions near the material maximum yield stress when considering the second scenario of load application (as abovementioned in chapter 4). By altering the material to Ti6Al4V ELI, the stress levels were reduced. However, due to the high density levels of the new material, component mass increased. Therefore, geometric changes were required to reduce weight while maintaining structural integrity and low stress levels.

Prototypes 1 and 2 integrated a complex geometry with thin walls leading to a large mass decrease (50%). However, considering the high rigidity titanium alloy, both prototypes 1 and 2 were prone to brake due to high stress areas where maximum stress occurs, as shown in figure 5.4.

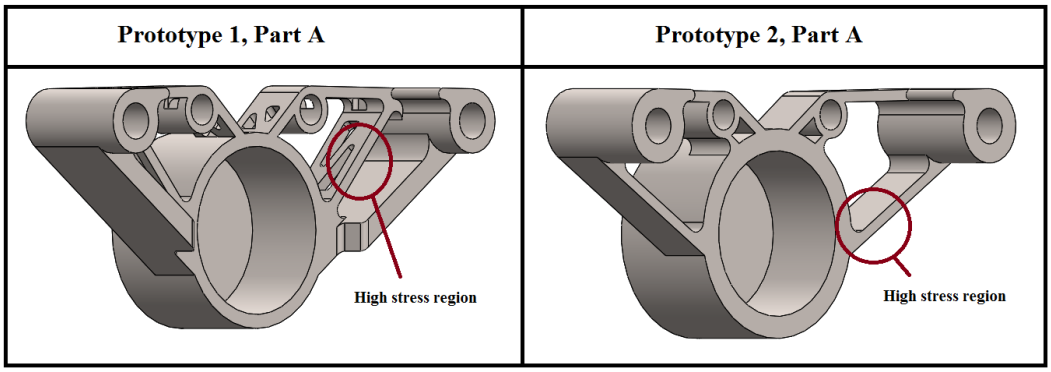

Figure 5.4- Prototype 1 and 2, part A.

To solve the localized stress problem, a different design was used in Prototype 3. The no-material areas were maintained however wall geometry was changed to address the high stress problem. Some changes were made to Prototype 3 to allow for its real-world utilization (O-ring cases, brake fluid canal, pad attachment points). Prototype 3 is presented in figure 5.5.

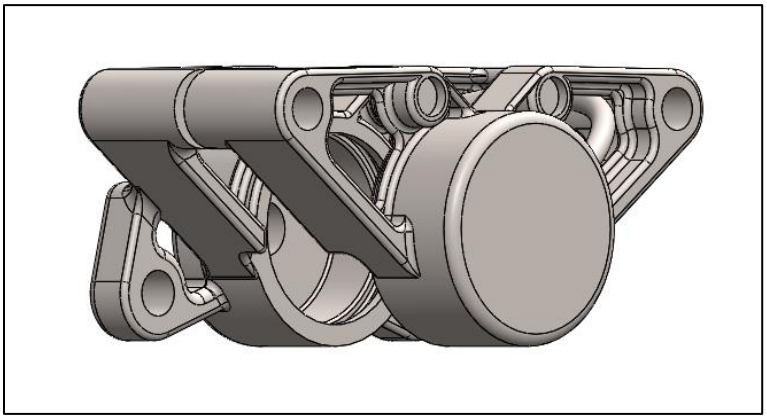

Figure 5.5- Prototype 3, parts A and B.

The changes made while redesigning Prototype 3 had in mind a decrease in overall components mass, being mass reduction an important goal for the design stage. Therefore,

before continuing with the study it is important to understand how the prototype mass compares to the original component mass. Computer software allows for mass determination based on material density and component volume. The original component was weighted to compare with results obtained by the software (See Figure 5.6).

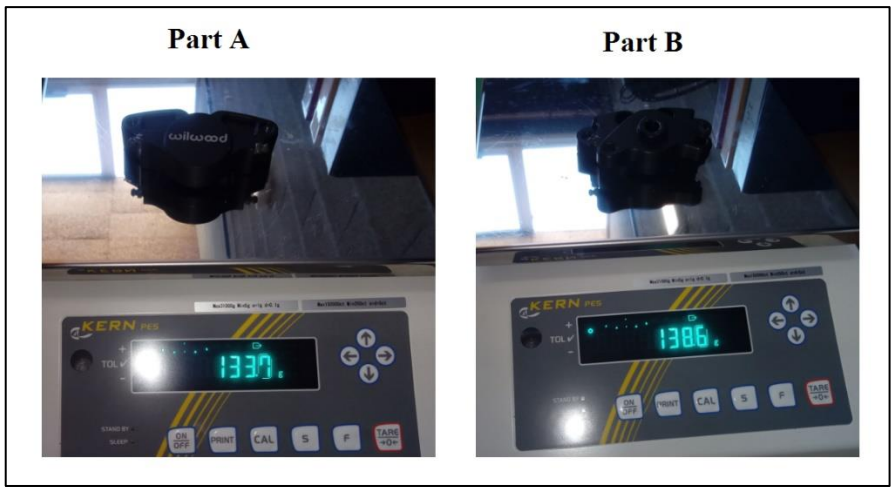

Figure 5.6- Original calliper assembly mass measurement.

According to physical measures, the original assembly, produced from grade 6 aluminium alloy has 272.3 g of mass. According to software, the original assembly has a mass of 270.3 g, allowing a model representation with 0.7 % relative error.

Prototype 3 mass must not overcome the original component mass to be set as valid for further analysis. Table 5.1 presents the real and simulated components mass.

Table 5.1- Original component and Prototype 3 mass determination

	Part A	Part B	Original Assembly	Prototype 3 A	Prototype 3 B	Prototype 3 Assembly
Real Mass (g)	133.7	138.6	272.3	NA	NA	NA
Simulated Mass (g)	132.1	138.2	270.3	100.7	120.6	221.3
Error Percentage	1.2	0.3	0.7	NA	NA	NA

According to initial simulations, Prototype 3 assembly represents an 18% mass decrease when compared to the original calliper assembly. Therefore, Prototype 3 is set as valid and further analysis can be conducted.

5.2. Static Study

It is of extreme importance to conduct a static study in Prototype 3 to understand its liabilities and if it represents an improvement when compared to the original component. Study

conditions applied to Prototype 3 must be the same as the ones applied to the original component.

Part A3 from Prototype 3 is attached to part B through two M8 bolts (attachment points A3.1 and A3.2). Constrains were applied in those points. Tangential force and hydraulic pressure were applied inside the cylinder case. See figure 5.7.

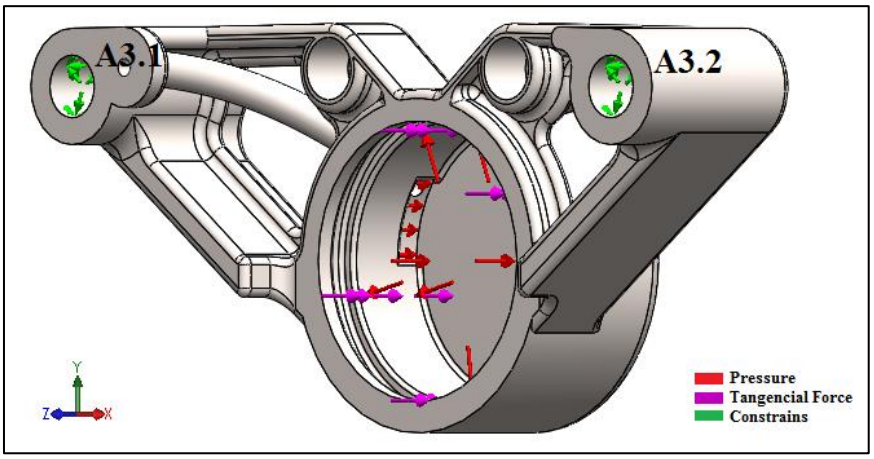

Figure 5.7- Prototype 3, part A3, loads and constrains.

Part B3 is attached to the vehicle´s sleeve through attachment points B3.3 and B3.4, similarly to B3 and B4 from the original component. Tangential force and hydraulic pressure were once more applied inside the cylinder case. Attachment points B3.1 and B3.2 are responsible for the load transfer from part A3, as shown in figure 5.8.

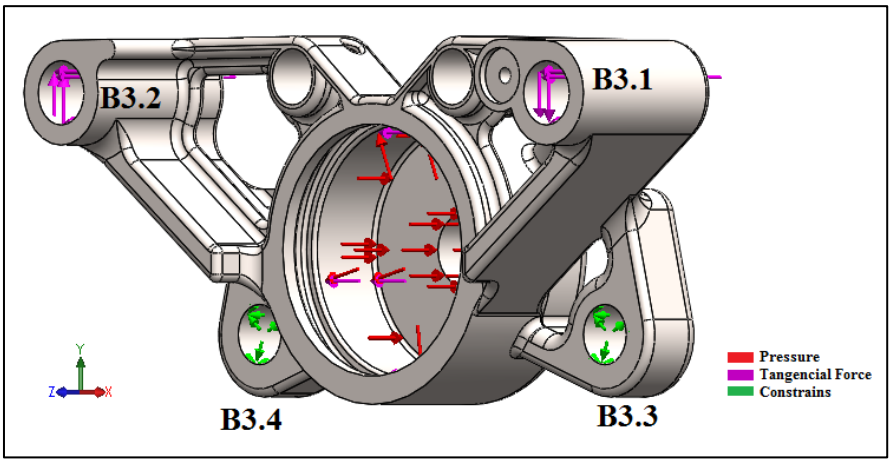

Figure 5.8- Prototype 3, part B3, loads and constrains

Prototype 3 load and constrain application points were the same as for the original component. According to chapter 3, study scenarios are as follows:

Scenario 1: While braking, the maximum brake pressure for stopping the vehicle without wheel lock occurring is generated considering a safety factor of 1.5 (67 bar).

Scenario 2: While braking, in a panic situation, the driver imposes a force of 2 kN (the maximum force that the brake system must withstand without brake failure occurring, according to regulations) to the brake pedal, generating maximum brake pressure (115 bar) [27].

For both scenarios, a maximum tangential force of 5938.97 N acting on the calliper was considered.

5.2.1. Scenario 1

As explained before, to compare simulation results it is important for Prototype 3 static analysis to be conducted following the same procedures as the original component static analysis.

For the first part (Part A3), load conditions and constraints were applied to run static simulations. 2970 N of tangential force and 67 bar of fluid pressure act inside the cylinder case while the part is constrained in attachment points A3.1 and A3.2. Static simulation results are presented in figure 5.9.

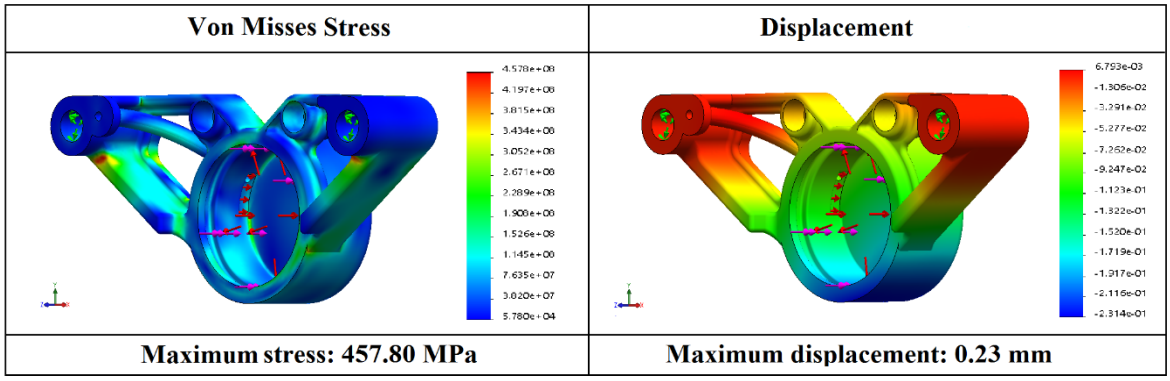

Figure 5.9- Part A3, scenario 1 simulation results.

According to von Misses criterion, the maximum stress on the component is of 457.80 MPa, located bellow the attachment points A3.1 and A3.2. This value is lower than the maximum material yield stress of 827.4 MPa. Meaning that the component will not plastically deform. Maximum displacement occurs in the cylinder case lower region with a maximum value of 0.23 mm.

For part B3 constrains were applied in attachment points B3.3 and B3.4 representative of the connection between calliper and vehicle sleeve. The load conditions were applied inside the cylinder case, in the same way as for part A3, however it was necessary to apply the loads imposed by part A3, acting on the attachment points B3.1 and B3.2. Simulation results are presented in figure 5.10.

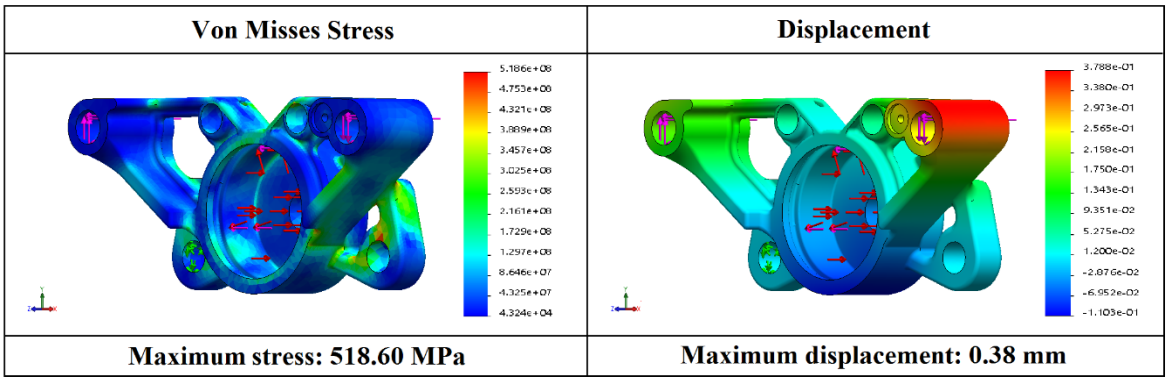

Figure 5.10- Part B3, scenario 1 simulation results.

Maximum von Misses stress occurs near the attachment point B3.3, with a maximum value of 518.60 MPa, once more, lower than the maximum material yield stress. Maximum displacement occurs along OZ axle, near attachment point B3.2, with a maximum value of 0.38 mm.

According to simulation results it is possible to conclude that Prototype 3 withstands the limit load conditions of a regular braking manoeuvre (scenario 1). However, scenario 1 does not consider a panic situation, therefore it is imperative to continue with Prototype 3 analysis to validate component design.

5.2.2. Scenario 2

Scenario 2 load application conditions are according formula student regulations, imposing a maximum force of 2 kN to the brake pedal. This is representative of a panic situation, where the driver pushes the pedal with maximum force. According to chapter 3, the force imposed to pedal assembly will translate in a maximum fluid pressure of 115 bar and 2970 N of tangential force [27].

For part A3 constrains were applied to attachment point A3.1 and A3.2. Tangential force and hydraulic pressure were applied inside the cylinder case, following previous static simulations.

After all variables considered the simulation was completed (See figure 5.11).

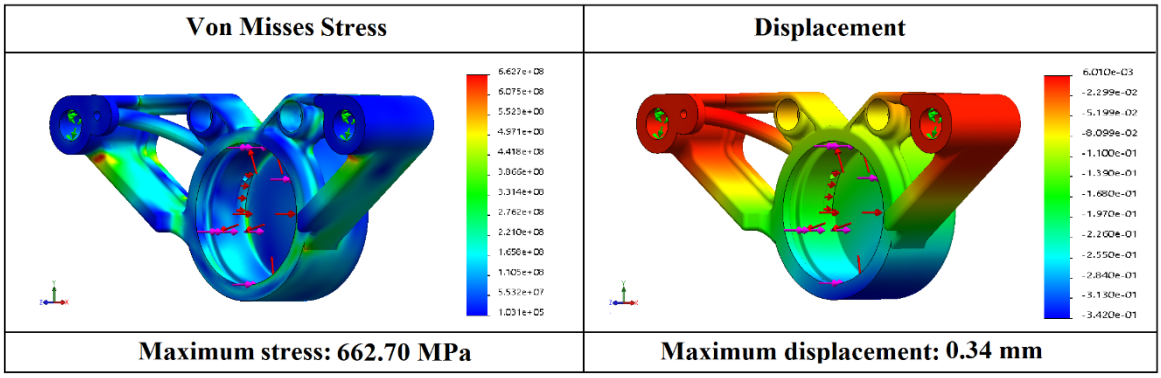

Figure 5.11- Part A3, scenario 2 simulation results.

According to von Misses criterion, maximum stress occurs bellow attachment points A3.1 and A3.2 with a maximum value of 662.70 MPa. Regarding maximum displacement it takes place on the lower region of the cylinder case, along OZ axle, with maximum value of 0.34 mm. Maximum von Misses stress is bellow maximum material yield stress of 827.40 MPa, meaning that plastic deformation will not occur.

For part B3 constrains were applied in attachment points B3.3 and B3.4, tangential force and hydraulic pressure on the cylinder case and, once more, the loads from part A3 were applied to attachment points B3.1 and B3.2.

After all variables considered the simulation was completed, see figure 5.12.

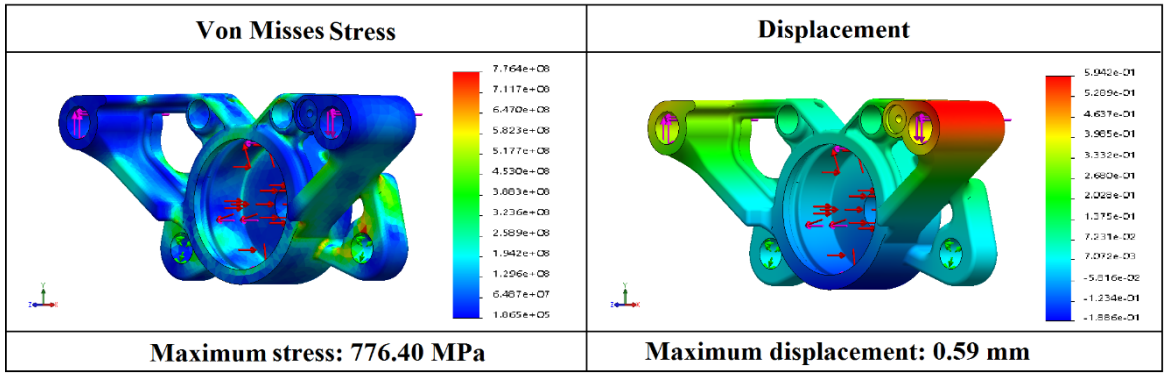

Figure 5.12- Part B3, scenario 2 simulation results.

Maximum von Misses stress occurs near attachment point B3.3 with a maximum value of 776.40 MPa, remaining inferior to maximum material yield stress of 827.40 MPa. Maximum displacement occurs near attachment point B3.1 along OZ axle with a maximum value of 0.59 mm.

5.2.3. Conclusions

The development of a new component is an iterative and time-consuming task. The search for a component design integrating low stress areas, easy component access for posterior maintenance and reduced material utilization can sometimes be an engineering challenge. Topological analysis comes as an alternative for the conventional component design process. It allows the definition of goals and constrains set by the user, based on a static study, creating new component designs that answer to the requirements imposed by the system.

After a topological simulation of the original brake calliper, using the new material (Ti6Al4V titanium alloy), a new geometry emerged, allowing for a better understanding of changes that could be made to reduce material utilization, therefore reducing component mass. Several component iterations were designed, based on topology study results, leading to a new component with less material utilization, Prototype 3.

To analyse Prototype 3 during braking, the same load conditions and constrains as the ones applied to the original component were considered (1st and 2nd scenario). During both 1st and 2nd scenarios of load application the von Misses stress distribution of Prototype 3 presented maximum values lower to maximum material yield stress. It means that Prototype 3 would maintain its structural integrity during utilization. Regarding maximum displacement, the values observed during simulation were not significant to limit piston travel or to cause system failure. Prototype 3 can therefore be set as valid and continue to production.

6. Production Stage

6.1. Prototype 3 production

Prototype 3 was designed to be produced using a titanium alloy (TiAl4V ELI, grade 23), however, there was a printer associated problem during the first stage of production that lead to the impossibility of full component production. Problem solution involved a new roller installation, which wasn´t available. At this point it was noticeable that a titanium alloy calliper wasn´t going to be produced in the timeframe available. To overcome this issue the possibility for manufacturing Prototype 3 using a different type of alloy emerged as a possible solution, validating the potential of AM redesigns to improve overall process and product sustainability.

To manufacture the new component, a steel alloy (Steel H13) was used, with the support of Centro de Desenvolvimento Rápito e Sustentado do Produto (CDRSP), a research unit of Polytechnic Institute of Leiria, and the effective production was done by a local company of the Additive Manufacturing market. The machine used to manufacture Prototype 3 was the EOSINT M280, illustrated in figure 6.1, with the specifications presented in table 6.1.

Table 6.1- Technical specifications for EOSINT M280, adapted from [33].

Characteristics	Specification
Laser type	Yb-fibre laser
Laser power	200 - 400 W
Diameter	100 – 500 µm
Power supply	32 A
Power consumption	8.5 kW (max)
Building volume	250x250x325 mm
Nitrogen generator	integrated
Compressed air supply	7.000hPa; 20m^3/h
Argon supply	4.000hPa; 100l/min

Figure 6.1- EOSINT M280, adapted from [33].

The stages involved in component production began with the STL type file obtained from the 3D computer model of the designed component as shown in figure 6.2. Using this file, it was possible to study possible iterations for an optimized component production.

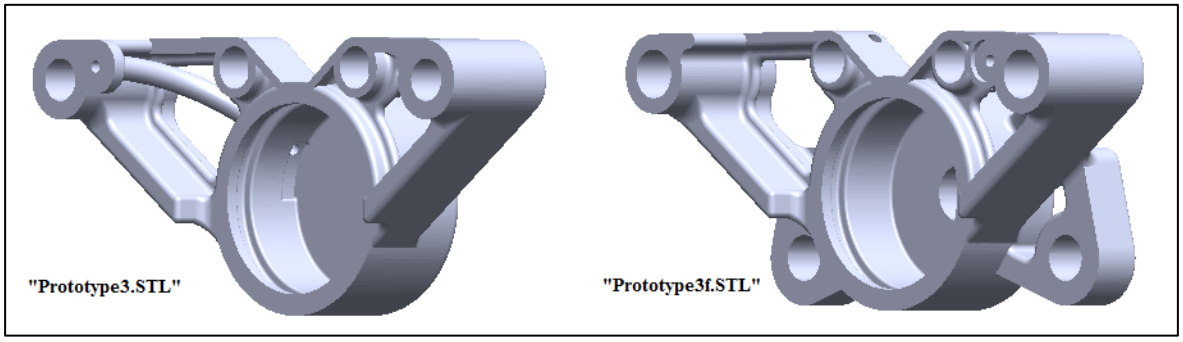

Figure 6.2- STL file from Prototype 3 design.

In the second stage of component production, support structures were added, and the component was placed in the building area using a specific software, 'Magics', for this application (see figure 6.3). This type of structures will support the material layers, and furthermore helping in the cooling of the melted material.

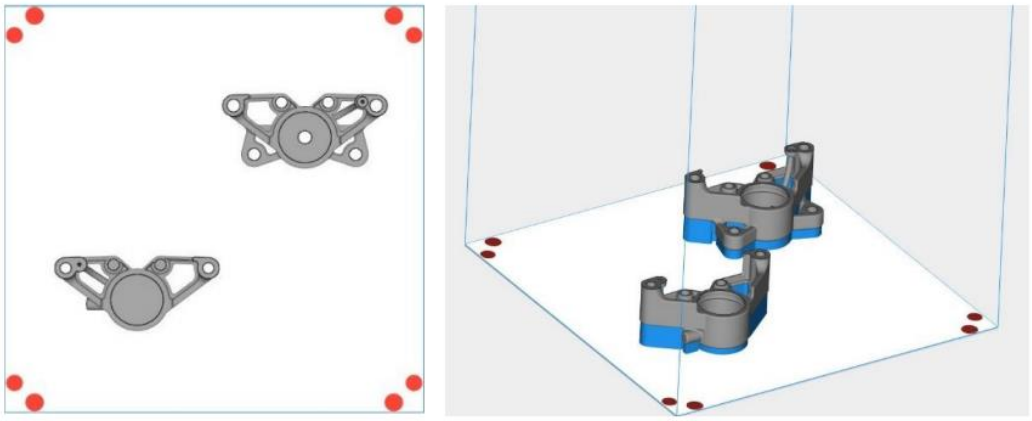

Figure 6.3- Component placement and support structures, Magics.

Following the creation of support structures and component placement, the file was saved as an SLM type file to begin the third stage of production. Through this file, the SLM production parameters were selected and the 3D model was sliced in layers with user defined thickness. During this stage of production, it is of extreme importance to correctly define production parameters to obtain the best results possible. A special attention must be given to laser power, scanning speed and component orientation.

6.2.Prototype 3 postproduction operations

The majority of components produced by Selective Laser Melting need a post printing heat treatment. During printing, melting of the powder metals leads to the formation of localized internal stresses. Heat treatments are used to eliminate residual stress on the components or to improve its mechanical characteristics. For the case in study, the heat treatment must be conducted in an atmosphere-controlled environment.

A stress relief process or any other heat treatment process conducted in a titanium alloy (Ti6Al4V for this study) must be conducted in vacuum conditions, According to Alessandro Fioresse, for the Ti6Al4V titanium alloy [34].

Sand blasting operations are also a post-printing process, usually conducted to remove excess material from the support structures and to improve surface quality. Sand blasting must be executed before any type of heat treatment.

Post printing processes also include machining and drilling to assure dimension compliance. During printing stage, the heat generated to melt the powder may cause localized deformations, leading to different dimensions from the original model. A common solution for this problem is to design the component with over thickness to machine it after production. This solution was used for Prototype 3 production. Drilling and threading must be conducted after Prototype 3 printing, in the point highlighted in figure 7.1.

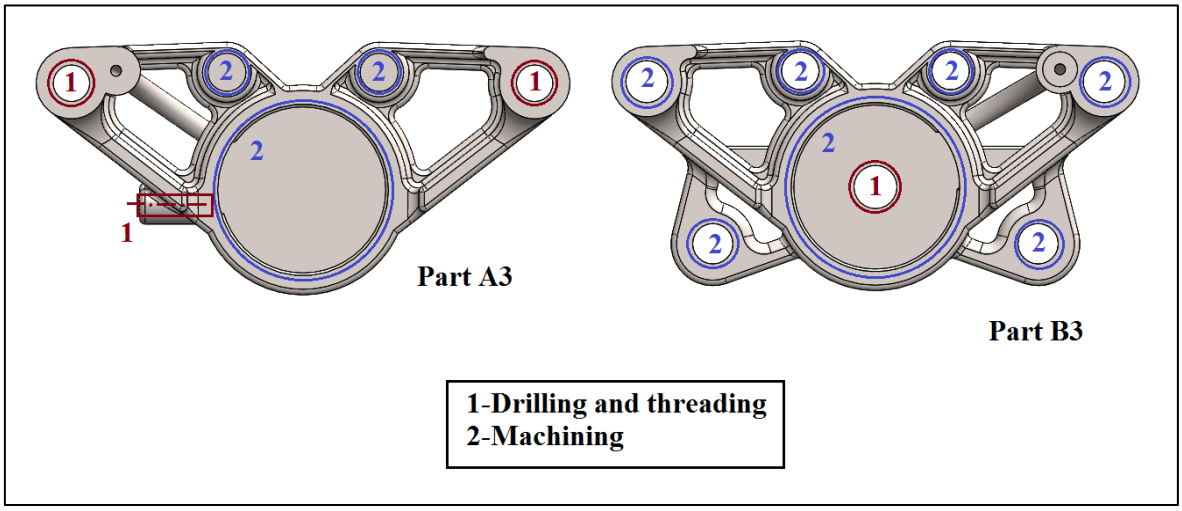

Figure 6.4- Post printing operations, Prototype 3.

Drilling, threading, and machining processes was performed in Prototype 3 according the figure presented above. Over thickness in those regions was considered in order not to remove excess material leading to dimension inaccuracy. Contact surfaces, O-ring and seal cases are not visible in figure 7.1, nevertheless also need machining to guaranty system safety and functionality.

Even though it was impossible to produce Prototype 3 using the desired titanium alloy, and a geometrical identic component was produced using a steel alloy (chapter 6). Several post-printing operations were conducted in this component to allow its utilization.

After component production a sand blasting operation was conducted to remove excess material and improve surface quality, as shown in figure 7.2.

Figure 6.5- Prototype 3, H13 Steel, after sand blasting.

After the sand blasting, drilling and threading operations took place to assure the connection between both parts of the calliper assembly, as represented in figure 7.3.

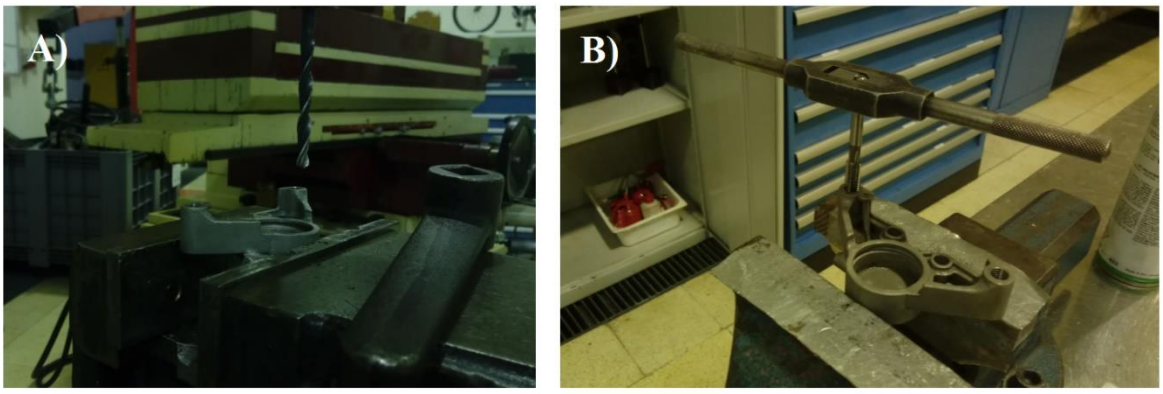

Figure 6.6- A) Prototype 3 drilling. B) Prototype 3 threading.

All drilling and threading operations are according figure 7.1.

Finalizing post-printing operations, an additional machining process is required to assure surface quality in the contact surfaces between both parts and inside the cylinder cases, preventing the braking fluid from leaking and assuring constant fluid pressure in the entire braking system.

The final component is presented in figure 7.4.

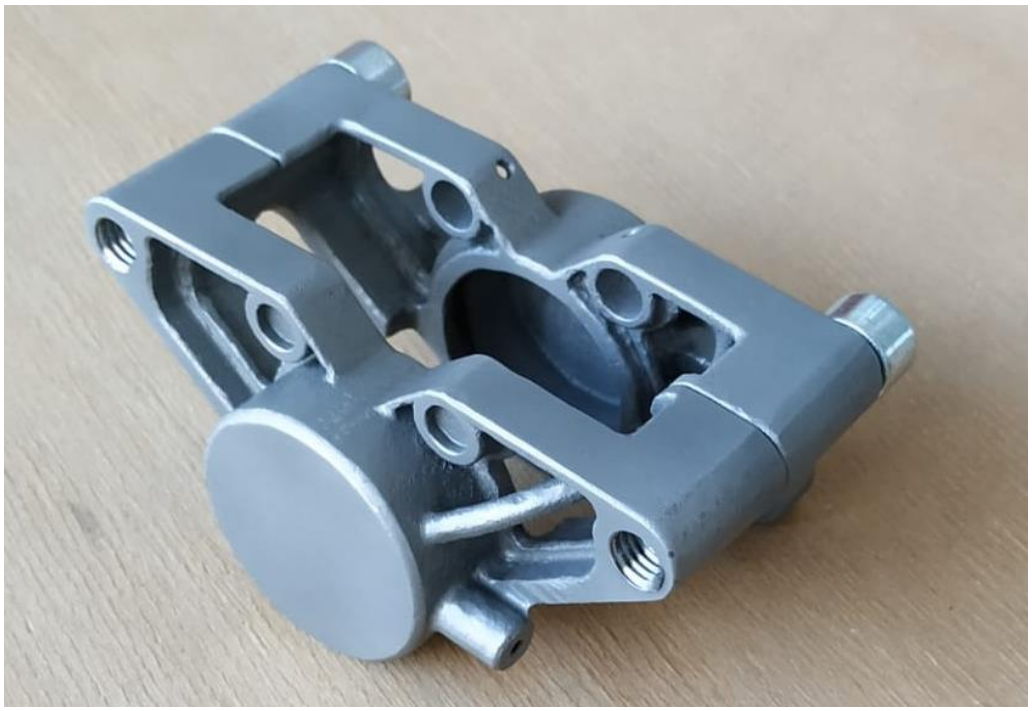

Figure 6.7- Prototype 3 assembly.

7. Final Conclusions and Future Improvements

Finalizing the present project, it is important to remember the main goals and prospect possible future improvements.

Bibliographic research allowed the presentation of different additive manufacturing families and processes, and how they´re positioned in the nowadays markets. The present project is focused on the metal additive manufacturing process. Therefore, metal AM processes were extensively explored to understand advantages and limitations of each process. After a careful analysis, the SLM process was selected as the most suitable for the project´s needs.

Regarding brake system study, it was conducted to be applicable to formula student type vehicles. Meaning that it can serve as a base for component selection, vehicle improvement and as a reference to future team members. Concluding the brake system study, maximum system loads (tangential force and brake pressure at the callipers) were determined for component development and testing.

The first computer static analysis was conducted using the original (wilwood) brake calliper. First results served as a validation method for the process used and as a reference for future static analysis. Concluding initial studies, it was possible to notice that the wilwood component was capable to deal with the loads and constrains imposed by the system without failure occurring. However, there was also noticeable localized stress regions with maximum values near the material's maximum yield stress. A component redesign using a different material was the approach chosen a possible solution.

Prototype stage began with the conclusions from the original component study, with the intent of developing a new component using less material while maintaining structural integrity. A new titanium alloy was chosen as the material for the new component, due to its mechanical characteristics and ability to be used in the SLM process. A topological study was conducted using this new material to understand possible component improvements. Three prototypes were obtained and analysed. Prototype 3 was the most promising and therefore selected for further analysis.

Prototype 3 was analysed using the same study conditions as for the original component to obtain comparable results. After completing simulations, it was possible to establish that Prototype 3, when compared to the original component, presented better mechanical characteristics and a significant reduction in mass.

Following Prototype 3 static study a new component was manufactured. Due to the impossibility of printing the component using the desired titanium alloy, a steel alloy was used. This new component served as a validation method for the design, proving that SLM technology allows the manufacturing of complex geometries and internal features with tight tolerances.

The final chapter presented the post printing processes required to make Prototype 3 usable. SLM technology allows for the component production, however a series of post-printing processes are required to allow the component implementation in the brake system.

Regarding future improvements it would be interesting to produce Prototype 3 using the desired titanium alloy to understand the advantages in mass reduction and component design. Furthermore, it would be prominent to implement Prototype 3 in the brake system for understanding its applicability.

Finalizing the present project, it is possible to conclude that SLM technology has evolved to the point that manufacturing a component which can serve as an improvement for an already existing system has become a real possibility. Constant improvements are being made to the SLM technology and it is expected to grow considerably in the following years, allowing for component production in the most diverse areas.

8. References

[1] Akebono, “akebono-brake,” 2020. [Online]. Available: https://www.akebono-brake.com/english/product_technology/product/automotive/disc/. [Accessed 09 April 2020].

[2] N. Aydin, “The realisation of CAD/CAM/CNC interoperabillity in prismatic part manufacturing,” University of Bath, 2007.

[3] C. Qiyi , B. P. Napolabel, P. Jerome O., M. Jill, C. A. Rigoberto and Leon, “Reactive and Funtional Polymers,” *High performance polymer nanocomposites for additive manufacturing applications,* pp. 141-155, 2016.

[4] C. Thomas, W. Christopher, I. Olga and G. Banning , “Could 3D Printing Change The World ?,” Atlantinc Council, 2011.

[5] F. G. Alpoim da Silva, “Comparação de Processos de Fabrico Aditivo,” FEUP, 2014.

[6] W. Di, Y. Yongqiang, Y. Ziheng and S. Xubin, “Research on the fabricating quality optimization of the overhanging surface in SLM process,” pp. 1471-1484, 23 June 2012.

[7] J. Cunningham, “The Additive Manufacturing Design Guide,” January 2017. [Online]. Available: https://www.eurekamagazine.co.uk/design-engineering-features/technology/the-additive-manufacturing-design-guide/149852/. [Accessed 02 June 2020].

[8] D. Bourell, J. Pierre, M. Leu, G. Levy, D. Rosen and A. Claire, “Manufacturing Technology,” *Material for additive manufacturing,* pp. 659-681, 09 April 2017.

[9] AMFG, “All you need to know about metal binder jetting,” AMFG, 03 07 2019. [Online]. Available: https://amfg.ai/2019/07/03/metal-binder-jetting-all-you-need-to-know/. [Accessed 15 September 2020].

[10] P. Kunchala, “3D printing high density ceramics using binder jetting with nanoparticle densifiers,” *Materials and Design,* vol. 155, 2018.

[11] “Additive Manufacturing,” AM, 2 3 2016. [Online]. Available: https://www.additivemanufacturing.media/articles/the-possibilities-of-electron-beam-additive-manufacturing. [Accessed 15 September 2020].

[12] Engineers Garage, “ENGINEERSGARAGE,” 20 7 2020. [Online]. Available: https://www.engineersgarage.com/tech-articles/3d-printing-processes-sheet-lamination-part-8-8/. [Accessed 15 September 2020].

[13] M. C. Thorsten Heeling, “Melt pool simulation for the evaluation of process parameters in selective laser melting,” *Additive Manufacturing,* vol. 14, pp. 116-125, 2017.

[14] J. Murphy, “ALL3DP,” ALL3DP, 28 03 2019. [Online]. Available: https://all3dp.com/2/selective-laser-melting-slm-3d-printing-simply-explained/. [Accessed 16 August 2020].

[15] P. Hanzl, M. Zetek and T. Baksa, “Science Direct,” *The Influence of Processing Parameters on the Mechanical Propreties of SLM Parts,* pp. 1406-1413, 2014.

[16] G. Dongdong and S. Yfu, “Aplied Surface Science,” *Processing conditions and microstructural features of porous 316L stainless steel components by DMLS,* pp. 1880-1887, 02 July 2008.

[17] G. Kai, W. Zemi, G. Ming, L. Xiangyou and Z. Xiaoyan, “Materials and Design,” *Effects of processing parameters on tensile properties of selective laser melted 304 stainless steel,* pp. 581-586, 2013.

[18] Y. S. Dongdoug Gu, “Balling phenomena in direct laser sintering of stainless steel powder,” pp. 2903-2910, 2009.

[19] T. Nikolay, M. Sergei , Y. Igor, L. Tahar, F. Ludo, T. Vitor and I. Michail, “Balling process puring seletive laser treatment of powders,” *Rapid Prototyping Journal,* vol. 10, no. 2, pp. 78-87, 2004.

[20] L. Ruidi, L. Jinhui, S. Ysheng, W. Li and J. Wei, “Balling behaviour of stainless steel and nickel powder during seletive laser melting process,” pp. 1025-1035, 2012.

[21] K. Rao, “Wind Energy for Power Generation,” Springer.

[22] S. Secrets, “Lateral and Longitudinal Loand Transfer,” 2019.

[23] AVON tyres motorsport, “SAE Formula Student,” AVON, 2019. [Online]. Available: http://www.avonmotorsport.com/resource-centre/tyre-applications/sae-formula-student. [Accessed 04 May 2020].

[24] Grove, “Aircraft Landing Gear Systems Inc.,” [Online]. Available: https://www.groveaircraft.com/torque.html. [Accessed 03 May 2020].

[25] P. Childs, “Mechanical Designs Engineering Handbook,” *Frictional Dynamics,* 2014.

[26] Nasi Auto Parts, “Friction coefficient of brake pads,” NAP, 2018. [Online]. Available: http://www.napbrake.com/2018/02/24/friction-coefficient-brake-pads/. [Accessed 02 May 2020].

[27] Formula Student Administration, Formula Student Rules, 2020.

[28] NASA (Kathy Johnson), “Human Performance Capabilities,” 2018.

[29] APRacing Ltd., “APRacing,” 2020. [Online]. Available: https://apracing.com. [Accessed 03 June 2020].

[30] e. Ádám Horváth, “Development of brake calliper for rally car,” 2012.

[31] Columbia University , Columbia Encyclopedia, New York: Columbia University Press, 2000-2006.

[32] SLM-Solutions, “Metal Powder,” SLM-Solutions Group AG, Germany, Lubeck, 2018.

[33] EOS, “Technical Description for EOSINT M280,” EOS, 2010.

[34] A. Fiorese, “Why heat treating materials after SLM manufacturing,” 10 09 2019. [Online]. Available: https://www.tav-vacuumfurnaces.com/blog/50/en/heat-treating-additive-manufacturing. [Accessed 12 August 2020].

[35] M. Loughead, “Fluid Operated Brakes”. Los Angeles California USA Patent 1,732,309, 23 May 1924.

[36] J. Rakshit, B. Vaibhav , M. Sharad and B. Chiranjeev, “A project on study and design of hydraulic braking system,” Indore, 2013.

[37] L. M. R. Seabra, “Design Optimization for Seletive Laser Melting and Experimental Testing of an Aicraft Component,” IST, Lisboa, 2015.

[38] S. Ford and M. Despeisse, “Additive manufacturing and sustainability: an exploratory study of the advantages and challenges,” *Journal of Cleaner Prodution,* vol. 137, pp. 1573-1587, 2016.

[39] P. Maldonaldo, Tese de Mestrado em utilização do fabrico aditivo no desenvolvimento de componentes da industria automovel, IPL, 2019.

[40] NASA, “Human Performance Capabilities,” 2020. [Online]. Available: https://msis.jsc.nasa.gov/sections/section04.htm. [Accessed 02 June 2020].

[41] Suspension Secrets, “Lateral and Longitudinal Load Transfer,” 2019. [Online]. Available: https://suspensionsecrets.co.uk/lateral-and-longitudinal-load-transfer/. [Accessed 02 May 2020].

[42] NASI, “NASI AutoParts,” 2018. [Online]. Available: http://www.napbrake.com/2018/02/24/friction-coefficient-brake-pads/. [Accessed 03 June 2020].

[43] Shop3D, “Shop3Dca,” Ultimaker, 2019. [Online]. Available: https://shop3d.ca/products/ultimaker-3-extended. [Accessed 19 June 2020].

[44] Wilwood engineering .inc, “Wilwood,” October 2020. [Online]. Available: https://www.wilwood.com/Calipers/CaliperProd?itemno=120-12178. [Accessed 12 November 2020].